The Dissertation Committee for Xiaochu Wang
certifies that this is the approved version of the following dissertation:

The Effect of Supercritical Fluid on Polymer Systems

Committee:

Isaac C. Sanchez, Supervisor

Roger T. Bonnecaze

Keith P. Johnston

Peter J Rossky

Thomas M. Truskett

The Effect of Supercritical Fluid on Polymer Systems

by

Xiaochu Wang, B.S.; M.S.

DISSERTATION

Presented to the Faculty of the Graduate School of

The University of Texas at Austin

in Partial Fulfillment

of the Requirements

for the Degree of

DOCTOR OF PHILOSOPHY

THE UNIVERSITY OF TEXAS AT AUSTIN

August 2007

To my wife Lingling,

My parents and my sister,

For their endless love, support and encouragement

Acknowledgments

First of all, I would like to express my deepest gratitude to my advisor, Dr. Isaac C. Sanchez for his guidance, advice and financial support. I thank him for his patient when I made a slow progress, and the many hours he spent with me on the discussion of technical problems, as well as writing of papers and this dissertation. Polymer physics was totally new research area to me when I joined his group, but his teaching, direction, inspiration and encouragement has helped me through and made this dissertation possible.

I also thank fellow group members Xiaoyan Wang, Ying Lu, Frank Willmore, David Simmons, Jianfang Zong for insightful discussions and sharing their ideas and experience.

I also want to express my sincere thanks to many people whom I have collaborated with on various projects. I thank Dr. Johnston and Yuan Li for the study of ordering in asymmetric block copolymer films by a compressible fluid. I thank Dr. Donald R. Paul and Yu Huang for the study of physical aging of thin glassy polymer films in terms of free volume. I thank Dr. Ekerdt and Kai Wu for the study of the effects of template on surfactant segregation in imprint lithography. I also want to thank my other committee members, Dr. Bonnecaze, Dr. Rossky, and Dr. Truskett for their all kinds of great help and advice.

My mother and father always encourage me to work hard and pursue my dream. I would also like to thank my wife for her love, understanding and encouragement. She has been sharing the pressures and joys with me for the last few years and I can not possibly thank her enough. The love and support from my wife, my parents and my sister has always been the source of my strength.

The Effect of Supercritical Fluid on Polymer Systems

Publication No. _____

Xiaochu Wang, Ph.D.
The University of Texas at Austin, 2007

Supervisor: Isaac C. Sanchez

Great interest has been directed toward the study of polymer thin films recently due to their emerging applications, and appreciable deviated properties and phenomena as compared with bulk polymers. Carbon dioxide (CO_2) has received attention as an environmentally benign alternative to hazardous industrial solvents. Unlike conventional liquid solvents, the density and hence the solvent strength of supercritical CO_2 can be tuned by small variations in pressure, temperature or both. The objective of this work is to study the interaction between high pressure CO_2 and polymer systems.

We introduced the methodology used in this dissertation. The combination of gradient theory of inhomogeneous systems and Sanchez-Lacombe Equation of State is used to calculate the interfacial properties, such as interfacial density profile, interfacial tension and interfacial thickness.

We first investigated the adsorption of supercritical fluid on polymer surfaces. We showed analytically that surface adsorption of high pressure fluid

on an attractive surface is proportional to the compressibility of the fluid. We have also investigated numerically the sorption of supercritical CO_2 on poly(dimethylsiloxane) (PDMS) and polyisobutylene (PIB), and supercritical 1,1-difluorethane on PS. By calculating the Gibbs adsorption and adsorption layer thickness of the supercritical fluids, we found in all cases that maximum adsorption occurred when the supercritical fluid was near its compressibility maximum.

We then examined the compatibilization effect of supercritical fluid on two incompatible polymers. We calculated the interfacial density profile, interfacial thickness and interfacial tension between the two polymers with and without the supercritical fluid. We found that the interfacial tension was decreased and the interfacial thickness was increased with high pressure supercritical fluid for the ternary systems we have investigated. No enhancement or deleterious effects on compatibilization were observed as the critical point was approached and the compressibility became large.

We also examined the morphological structures of asymmetric poly(ethylene oxide)-b-poly(1,1'-dihydroperflurooctyl methacrylate) (PEO-b-PFOMA) thin films upon annealing in supercritical CO_2. The strong affinity between PFOMA and CO_2 was found to induce phase segregation when annealing PEO-b-PFOMA films as compared with vacuum at the same temperature.

Table of Contents

List of Tables

List of Figures

Chapter 1

Introduction

1.1 Motivation and Research Objectives

A great deal of interest has been directed toward the study of polymer thin films due to their emerging applications, and appreciable deviated properties and phenomena as compared with bulk polymers. Polymer thin films are critical in many technological and industrial applications, ranging from dielectric coatings, membranes, resist layers for lithography, to device technologies such as polymer thin film transistors [1, 2]. These systems provide many advantages, including cost, processability and control of properties over other materials. Most films of interest are less than 10000 Å, and a range of phenomena in thin films can not be observed in their bulk counterpart [3–11]. The conflicting goals of reducing film thickness and improving film properties, e.g. uniformity, stability and adhesion to surfaces, require an understanding how materials properties, such as the glass transition temperature (T_g), chain dynamics and phase behavior of polymer blends or copolymers, are influenced by the thin film thickness as well as the interfacial interactions associated with interfaces.

Supercritical CO_2 has been studied extensively as a regeneration sol-

vent in a range of technical and chemical processes, such as chromatography, extraction, reactor cleanup, preparation of pharmaceutical products, polymer and semiconductor process [12–15]. CO_2 is an attracting solvent because it is abundant, non-toxic, and environmentally benign and has an easily accessible critical point. Besides, the solvent properties of CO_2, such as density, dielectric constant, viscosity and diffusivity can be finely tuned by small variations in pressure and/or temperature. Considerable attentions have been given to the topics related to polymer melts and CO_2. For example, the use of supercritical CO_2 can be seen in the processing of biodegradable/biocompatible polymers because of the low thermal stability of these polymers and the lack of organic solvents in processing them [13]. The tunable solvent properties render supercritical CO_2 a promising annealing medium to induce ordering in block copolymer thin film template. In addition, the low interfacial tensions in supercritical CO_2 enable its applications in processing wafers with high aspect ratio features to enhance solvent penetration and to avoid pattern collapse [16].

This dissertation investigates the interaction between supercritical fluid and polymer systems (polymer surfaces, polymer interfaces and block copolymer). First, the adsorption of supercritical fluid on attractive wall is examined theoretically, and the adsorption of supercritical fluid on polymer thin films is examined numerically. Second, we investigate the compatibilization effect of supercritical fluid on two incompatible polymers. Third, we examine the CO_2 induced phase segregation in PEO-b-PFOMA block copolymer films.

The following sections of this chapter are intended to provide a background and context for the work described in the body of this dissertation.

1.2 Critical Adsorption of Polymer Thin Films

An interesting anomalous sorption of CO_2 onto polymer thin films supported on the inorganic substrates, such as SiO_2 and GaAs, was reported by using in-situ spectroscopic ellipsometry [6] when CO_2 was near its critical point as shown in Figure 1.1. The maximum swelling ratio and a corresponding minimum in refractive index occur in regions of pressure where CO_2 is highly compressible. But, for CO_2-bulk polymer system, the swelling isotherm exhibits a characteristic sigmoidal shape [17, 18]. Similar maximum of swelling ratio was also found for CO_2-polymer thin films using in situ neutron reflectivity [7, 19]. The mechanism of the film thickening is unclear: it may be that the CO_2 is forming a liquid layer on the surface of the polymer film, or the CO_2 is absorbing into the film and swelling it.

1.3 Welding Polymers

Welding of polymers occurs when the polymer chains at the surface of one component are mobile enough to entangle with chains in the other component. Usually, thermal energy is applied to raise the temperature of the polymer above the appropriate transition temperature, i.e. the glass transition temperature, T_g, for amorphous thermoplastic polymers, or the melting temperature, Tm, for semi-crystalline polymers. Above these transition tem-

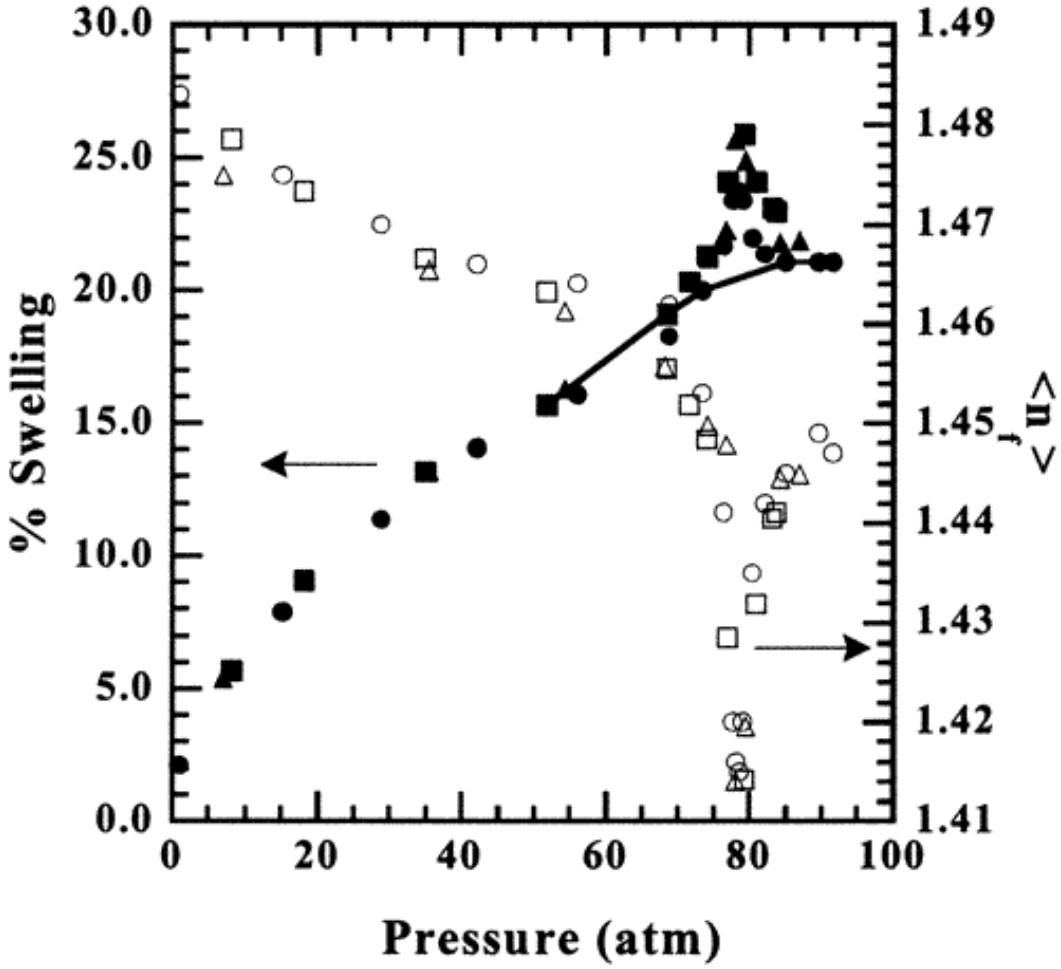

Figure 1.1: Swelling isotherms and average refractive indices of swollen PMMA thin film at 35 °C. Isotherms represent the first desorption runs. Filled symbols represent swelling isotherms, and corresponding open symbols represent refractive index isotherms. Circles represent h_0=88 nm on SiO_2, squares represent h_0=321 nm on SiO_2, and triangles represent h_0=89 nm on GaAs. The solid line represents the interpolated baseline swelling

peratures, polymer chains are mobile and if two components are brought into intimate contact, polymer chain entanglement will proceed, resulting in a weld. Polymer welding processes can be divide into three groups: 1) Processes involving mechanical movement: ultrasonic welding, friction welding, vibration welding. 2) Processes involving external heating: hot plate welding, hot gas welding and resistive and implant welding. 3) Processes involving adding compatibilizer, solvent or even another polymer.

In solvent welding, a solvent is applied which can temporarily dissolve the polymer at room temperature. When this occurs, the polymer chains are free to move in the liquid and can entangle with other similarly dissolved chains in the other component. Given sufficient time, the solvent will permeate through the polymer and out into the environment, so that the chains lose their mobility. This leaves a solid mass of entangled polymer chains which constitutes a solvent weld. Solvent welding has been employed extensively in applications such as manufacture of piping systems and for assembling toys. However, legislation designed to minimize industrial use of organic solvents is likely to impose limitations on use of solvent welding in the foreseeable future.

Much attention has been focused on the experimental and theoretical studies of polymer blends in the presence of solvent [20–28]. The interfacial thickness between the PS/PB polymer blend exposed to high pressure CO_2 was increased up to 100 Å even near room temperature, while the interfacial width without CO_2 exposure was at most 40 Å even at the highest temperature (T = 175 °C)[21]. Significant enhancement of the mechanical properties in PS/EVA

blends is achieved via supercritical CO_2 exposure in the pressure/temperature domain where the density fluctuation is maximal [27].

Molecular simulation of polymer welding has been very rare because of its complexity. A cubic F lattice model of dense polymer systems, implementing a kinetic Monte Carlo diffusion algorithm was used to simulate polymer welding [29, 30].

1.4 Block Copolymer

Block copolymers are comprised of two or more homopolymer subunits linked by covalent bonds. The union of the homopolymer subunits may require an intermediate non-repeating subunit, known as a junction block. Block copolymers with two or three distinct blocks are called diblock (Figure 1.2(a)) copolymers and triblock copolymers, respectively. Due to the incompatibility of the two block component, a diblock copolymer can phase segregated into A-rich and B-rich domains below its corresponding order-disorder transition (ODT) temperature. However, this phase segregation only occurs at nanometer length scales because of the imposed connectivity between the two blocks. Specifically, the scale of the self-assembled structure depends on the number of monomers, N, and segment size, a_0, and the strength of interaction between the blocks, represented by the Flory-Huggins interaction parameter, χ. The ordered morphology depends on the composition of the copolymer, represented by the volume fraction of one block, f. As the volume fraction goes from low value ($f \sim 0$) to high values ($f \sim 0.5$), the phase-segregated

(a)

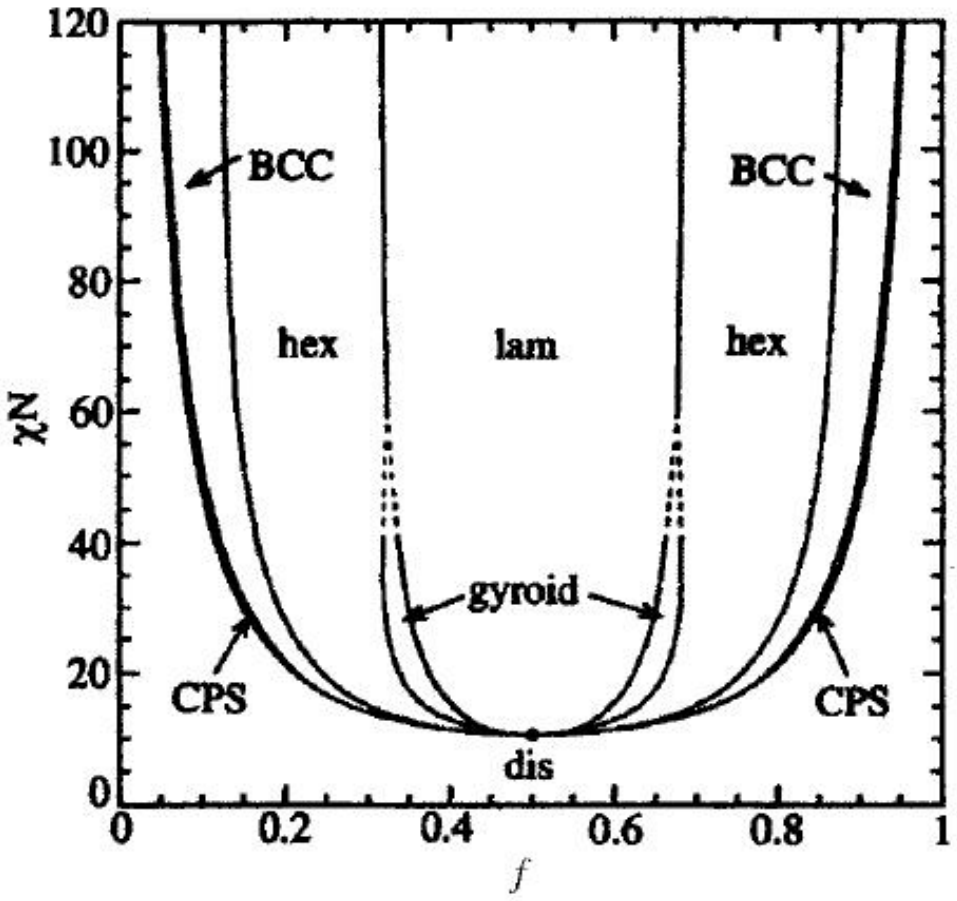

(b)

Figure 1.2: (a) Schematic drawing of and A-b-B diblock copolymer. (b) The mean-field theory calculated phase diagram of a typical diblock copolymer. Phase diagram are reproduced from The Physics of Block Copolymers

microstructures evolve from body-centered cubic arrays of spheres, to hexagonally packed cylinders, then to bicontinuous structures, and finally to lamellae. For each volume fraction, f, there is a critical χN above which the diblock will phase separate into its designated morphology. For instance, mean-field theory indicates that $(\chi N)_{\text{crit}} = 10.5$ for a symmetrical diblock copolymer ($f = 0.5$) and $(\chi N)_{\text{crit}} \sim 27$ for an asymmetrical diblock copolymer with $f = 0.15$.

In recent years, rapid progress has been reported toward exploiting microphase segregation in block copolymer (BCP) thin films to create periodically ordered nanopatterned substrates for potential applications such as nanolithography and "bottom" up microelectronic device fabrication [31, 32].

1.5 Dissertation Outline

This dissertation is devoted to understand the effects of high pressure CO_2 on the polymer systems by using computational methods.

In Chapter 2, we introduce the methodology used in this dissertation. The combination of gradient theory of inhomogeneous systems and Sanchez-Lacombe Equation of State is used to calculate the interfacial properties.

In Chapter 3, we examine the adsorption of supercritical fluid on polymer surfaces. We show analytically that surface adsorption on an attractive surface is proportional to the compressibility of the fluid. We have also investigated numerically the sorption of supercritical CO_2 on PDMS and PIB, and supercritical 1,1-difluoroethane on PS. By calculating the Gibbs adsorption

and adsorption layer thickness of the supercritical fluids, we find in all cases (different substrates, different supercritical fluids) that maximum adsorption occurs when the supercritical fluid is near its compressibility maximum.

In Chapter 4, we examine the compatibilization effect of supercritical fluid on two incompatible polymers. We calculate the interfacial density profile, interfacial thickness and interfacial tension between the two polymers with and without the supercritical fluid. We find that the interfacial tension is decreased and the interfacial thickness is increased with high pressure supercritical fluid for the ternary systems we have investigated. No enhancement or deleterious effects on compatibilization are observed as the critical point is approached and the compressibility becomes large.

In Chapter 5, we examine the morphological structures of asymmetric PEO-b-PFOMA thin films upon annealing in supercritical CO_2. The strong affinity between PFOMA and CO_2 is found to induce phase segregation when annealing PEO-b-PFOMA films as compared with vacuum annealing at the same temperature. The results are explained based on the relative interaction parameters, $\chi_{\mathrm{PFOMA-CO_2}}$ and $\chi_{\mathrm{PEO-CO_2}}$.

In the last chapter, we summarize our work and suggest future research.

1.6 Bibliography

[1] Cintavey, L. A.; Clarson, S. J.; Husband, D. M.; De Brabander, G. N.; Boyd, J. T. *Journal of Applied Polymer Science* **2000**, *76*(9), 1448–1456.

[2] Ziemelis, K. *Nature* **1998**, *393*(6686), 619–620.

[3] Frank, C. W.; Rao, V.; Despotopoulou, M. M.; Pease, R. F. W.; Hinsberg, W. D.; Miller, R. D.; Rabolt, J. F. *Science* **1996**, *273*(5277), 912–915.

[4] Sirard, S. M.; Green, P. F.; Johnston, K. P. *Journal of Physical Chemistry B* **2001**, *105*(4), 766–772.

[5] Sirard, S. M.; Gupta, R. R.; Russell, T. P.; Watkins, J. J.; Green, P. F.; Johnston, K. P. *Macromolecules* **2003**, *36*(9), 3365–3373.

[6] Sirard, S. M.; Ziegler, K. J.; Sanchez, I. C.; Green, P. F.; Johnston, K. P. *Macromolecules* **2002**, *35*(5), 1928–1935.

[7] Koga, T.; Seo, Y. S.; Shin, K.; Zhang, Y.; Rafailovich, M. H.; Sokolov, J. C.; Chu, B.; Satija, S. K. *Macromolecules* **2003**, *36*(14), 5236–5243.

[8] Green, P. F. *Journal of Polymer Science Part B-Polymer Physics* **2003**, *41*(19), 2219–2235.

[9] Pham, J. Q.; Green, P. F. *Macromolecules* **2003**, *36*(5), 1665–1669.

[10] Besancon, B. M.; Soles, C. L.; Green, P. F. *Physical Review Letters* **2006**, *97*(5).

[11] Arceo, A.; Green, P. F. *Journal of Physical Chemistry B* **2005**, *109*(15), 6958–6962.

[12] McHugh, M. A.; Krukonis, V.; 2nd ed., 1994.

[13] Tomasko, D. L.; Li, H. B.; Liu, D. H.; Han, X. M.; Wingert, M. J.; Lee, L. J.; Koelling, K. W. *Industrial and Engineering Chemistry Research* **2003**, *42*(25), 6431–6456.

[14] Nalawade, S. P.; Picchioni, F.; Janssen, L. *Progress in Polymer Science* **2006**, *31*(1), 19–43.

[15] Yeo, S. D.; Kiran, E. *Journal of Supercritical Fluids* **2005**, *34*(3), 287–308.

[16] Zhang, X. G.; Pham, J. Q.; Ryza, N.; Green, P. F.; Johnston, K. P. *Journal of Vacuum Science and Technology B* **2004**, *22*(2), 818–825.

[17] Shim, J. J.; Johnston, K. P. *Aiche Journal* **1989**, *35*(7), 1097–1106.

[18] Fleming, G. K.; Koros, W. J. *Macromolecules* **1986**, *19*(8), 2285–2291.

[19] Koga, T.; Seo, Y.-S.; Zhang, Y.; Shin, K.; Kusano, K.; Nishikawa, K.; Rafailovich, M. H.; Sokolov, J. C.; Chu, B.; Peiffer, D.; Occhiogrosso, R.; Satija, S. K. *Physical Review Letters* **2002**, *89*(12), 125506/1–125506/4.

[20] Yoon, K. S.; Pak, H.; Lee, J. W.; Chang, T. *Bulletin of the Korean Chemical Society* **1994**, *15*(3), 214–221.

[21] Koga, T.; Jerome, J. L.; Seo, Y. S.; Rafailovich, M. H.; Sokolov, J. C.; Satija, S. K. *Langmuir* **2005**, *21*(14), 6157–6160.

[22] Walker, T. A.; Raghavan, S. R.; Royer, J. R.; Smith, S. D.; Wignall, G. D.; Melnichenko, Y.; Khan, S. A.; Spontak, R. J. *Journal of Physical Chemistry B* **1999**, *103*(26), 5472–5476.

[23] Walker, T. A.; Melnichenko, Y. B.; Wignall, G. D.; Spontak, R. J. *Macromolecules* **2003**, *36*(12), 4245–4249.

[24] Walker, T. A.; Colina, C. M.; Gubbins, K. E.; Spontak, R. J. *Macromolecules* **2004**, *37*(7), 2588–2595.

[25] Li, H. B.; Lee, L. J.; Tomasko, D. L. *Industrial and Engineering Chemistry Research* **2004**, *43*(2), 509–514.

[26] Koga, T.; Jerome, J.; Rafailovich, M. H.; Chu, B.; Douglas, J.; Satija, S. *Advances in Colloid and Interface Science* **2006**, *128*, 217–226.

[27] Palermo, E.; Si, M.; Occhiogrosso, R.; Berndt, C.; Rudomen, G.; Rafailovich, M. *Macromolecules* **2005**, *38*(22), 9180–9186.

[28] Hong, K. M.; Noolandi, J. *Macromolecules* **1981**, *14*(3), 736–742.

[29] Anderson, K. L.; Wescott, J. T.; Carver, T. J.; Windle, A. H. *Materials Science and Engineering a-Structural Materials Properties Microstructure and Processing* **2004**, *365*(1-2), 14–24.

[30] Haire, K. R.; Windle, A. H. *Computational and Theoretical Polymer Science* **2001**, *11*(3), 227–240.

[31] Segalman, R. A. *Materials Science and Engineering R-Reports* **2005**, *48*(6), 191–226.

[32] Fasolka, M. J.; Mayes, A. M. *Annual Review of Materials Research* **2001**, *31*, 323–355.

Chapter 2

Methodology

The combination of gradient theory of inhomogeneous systems and Sanchez-Lacombe Equation of State is used to calculate the surface properties, and the two theories are introduced in the following two sections.

2.1 Gradient Theory of Inhomogeneous Systems

The interfacial tension, γ, for a planar interface can be defined as

$$\gamma = (A - A_e) / S_0 \tag{2.1}$$

where S_0 is the surface area, A is the inhomogeneous systems Helmholtz free energy, and A_e, is the Helmholtz free energy of a hypothetical homogeneous system of the same density and composition. In order to evaluate A, we adopt the standard assumption [1], that the entropy of the inhomogeneous system is only a function of the local density and independent of density gradients. For polymer molecules, the validity of this assumption is expected to be limited.

Effects of density gradients on the potential energy, E, are evaluated in a mean-field approximation. The potential energy per unit volume, V, and position R for an n-component system with pairwise additive interactions can

be written as

$$E\left(\mathrm{R}\right)/V = (1/2)\sum_{i}^{n}\sum_{j}^{n}\epsilon_{ij}\left(\mathrm{R}\right) \tag{2.2}$$

where ϵ_{ij} is the interaction energy of components i and j and is given by

$$\epsilon_{ij}\left(\mathrm{R}\right) = \rho_i\left(\mathrm{R}\right)\int \rho_j\left(\mathrm{R}+\mathrm{s}\right)u_{ij}\left(\mathrm{s}\right)d\mathrm{s} \tag{2.3}$$

ρ_i and ρ_j are the densities of components i and j, $s = |\mathrm{s}|$ is the intermolecular distance, and u_{ij} is the intermolecular interaction potential, which is assumed to be spherically symmetric. Now $\rho_j\left(\mathrm{R}+\mathrm{s}\right)$ is expanded in a Taylor series around $\mathrm{s} = 0$

$$\rho_j\left(\mathrm{R}+\mathrm{s}\right) = \rho_j\left(\mathrm{R}\right) + \left(\nabla\rho_j\cdot\mathrm{s}\right) + \frac{1}{2!}\left(\nabla\rho_j\cdot\mathrm{s}\right)^2 + \cdots \tag{2.4}$$

Substitution of equation 2.4 into equation 2.3 and subsequent integration yields

$$\varepsilon_{ij}\left(\mathrm{R}\right) = -\rho_i\left(\mathrm{R}\right)\rho_j\left(\mathrm{R}\right)\kappa_0^{ij} + \rho_i\left(\mathrm{R}\right)\int\left\{\left(\nabla\rho_j\cdot\mathrm{s}\right) + \left(1/2\right)\left(\nabla\rho_j\cdot\mathrm{s}\right)^2 + \cdots\right\}u_{ij}\left(\mathrm{s}\right)d\mathrm{s} \tag{2.5}$$

with

$$\kappa_0^{ij} = -4\pi\int_{\sigma_{ij}}^{\infty}\mathrm{s}^2 u_{ij}\left(\mathrm{s}\right)d\mathrm{s} \tag{2.6}$$

where σ_{ij}^3 is the repulsive core volume between components i and j . Since u_{ij} is spherically symmetric, it is an even function of s_x, s_y, and s_z, so that the integral in equation 2.5 has the following properties for odd b:

$$\int\left(\nabla\rho_j\cdot\mathrm{s}\right)^b u_{ij}\left(\mathrm{s}\right)d\mathrm{s} = 0 \tag{2.7}$$

After integration equation 2.5 becomes

$$\varepsilon_{ij}\left(\mathrm{R}\right)=-\rho_{i}\left(\mathrm{R}\right)\rho_{j}\left(\mathrm{R}\right)\kappa_{0}^{ij}-\rho_{i}\left(\mathrm{R}\right)\nabla^{2}\rho_{j}\left(\mathrm{R}\right)\kappa_{2}^{ij}+\cdots \tag{2.8}$$

with

$$\kappa_{2}^{ij}=-\left(2\pi/3\right)\int_{\sigma_{ij}}^{\infty}\mathrm{s}^{4}u_{ij}\left(\mathrm{s}\right)d\mathrm{s} \tag{2.9}$$

Neglecting fourth and higher order terms in equation 2.8 is the usual gradient approximation. Defining the local Helmholtz free energy density $a_0(\mathrm{R})$ as

$$a_{0}\left(\mathrm{R}\right)=-\left(1/2\right)\sum_{i}\sum_{j}\rho_{i}\left(\mathrm{R}\right)\rho_{j}\left(\mathrm{R}\right)\kappa_{0}^{ij}-TS\left(\rho_{1},\rho_{2},\cdots,\rho_{n}\right) \tag{2.10}$$

where T is the temperature and S is the entropy per unit volume, results in the following expression for the Helmholtz free energy density of an inhomogeneous system:

$$a\left(\mathrm{R}\right)=a_{0}\left(\mathrm{R}\right)-\left(1/2\right)\sum_{i}\sum_{j}\rho_{i}\left(\mathrm{R}\right)\rho_{j}\left(\mathrm{R}\right)\kappa_{0}^{ij} \tag{2.11}$$

The total Helmholtz free energy for a system with a planar interface of area S_0 and volume LS_0 is

$$A=S_{0}\int_{-L/2}^{L/2}\left[a_{0}\left(x\right)+\left(1/2\right)\sum_{i}\sum_{j}\rho_{i}\left(x\right)\frac{d^{2}\rho_{j}\left(x\right)}{dx^{2}}\kappa_{2}^{ij}\right]dx \tag{2.12}$$

Integration by parts of the second term in the integral leads to further simplification ($d\rho_i/dx \to 0$ as $L \to \infty$)

$$A=S_{0}\int_{-L/2}^{L/2}\left[a_{0}\left(x\right)+\left(1/2\right)\sum_{i}\sum_{j}\left(\frac{d\rho_{i}}{dx}\right)\left(\frac{d\rho_{j}}{dx}\right)\kappa_{2}^{ij}\right]dx \tag{2.13}$$

The final expression for the interfacial tension is

$$\gamma=\int_{-\infty}^{\infty}\left[\Delta a+\left(1/2\right)\sum_{i}\sum_{j}\left(\frac{d\rho_{i}}{dx}\right)\left(\frac{d\rho_{j}}{dx}\right)\kappa_{2}^{ij}\right]dx \tag{2.14}$$

where

$$\Delta a = a_0(x) - A_e/V = a_0(x) - \sum_i \rho_i(x)\,\mu_i^e + P_e \tag{2.15}$$

μ_i^e is the equilibrium chemical potential and P_e is the external pressure.

Minimization of equation 2.14 yields n-coupled differential equations (Euler-Lagrange equations)

$$\begin{gathered}\frac{\partial \Delta a}{\partial \rho_i} - (1/2)\sum_j \kappa_2^{ij}\frac{d^2\rho_j}{dx^2} = 0 \\ i = 1, 2, \cdots, n\end{gathered} \tag{2.16}$$

Multiplying the differential equations by $d\rho_i/dx$ and summing over species i yields

$$\frac{d}{dx}\left[\Delta a - (1/2)\sum_i\sum_j \kappa_2^{ij}\left(\frac{d\rho_i}{dx}\right)\left(\frac{d\rho_j}{dx}\right)\right] = 0 \tag{2.17}$$

which upon integration yields

$$\Delta a = (1/2)\sum_i\sum_j \kappa_2^{ij}\left(\frac{d\rho_i}{dx}\right)\left(\frac{d\rho_j}{dx}\right) \tag{2.18}$$

The equilibrium tension can thus be expressed as

$$\gamma = \sum_i\sum_j \kappa_2^{ij}\int_{-\infty}^{\infty}\left(\frac{d\rho_i}{dx}\right)\left(\frac{d\rho_j}{dx}\right)dx = 2\int_{-\infty}^{\infty}\Delta a\,dx \tag{2.19}$$

Equation 2.19 was first derived by Bongiorno, Scriven, and Davis [2] by a different procedure. For a single component these equations reduce to the well-known Cahn-Hilliard equations [1]. The derivation given above is quite general, and the resulting expression for the interfacial tension can be applied

to any mean-field fluid model which provides an expression for the equilibrium chemical potential and a specific form of the intermolecular interaction potential.

2.2 Sanchez-Lacombe (S-L) Equation of State

The lattice fluid equation of state describes density dependent phenomena by incorporating vacant sites [3]. The S-L equation of state is given by:

$$\tilde{\rho}^2 + \tilde{P} + \tilde{T}\left[\ln\left(1-\tilde{\rho}\right) + \left(1-\frac{1}{r}\right)\tilde{\rho}\right] = 0 \tag{2.20}$$

where $\tilde{T}$, $\tilde{P}$, $\tilde{\rho}$ are reduced temperature, pressure and density, respectively. The reduced variables are defined in terms of characteristic parameters:

$$\begin{array}{ll} \tilde{T} = T/T^* & T^* = \epsilon^*/R \\ \tilde{P} = P/P^* & P^* = \epsilon^*/v^* \\ \tilde{\rho} = \rho/\rho^* & \rho^* = M/\left(rv^*\right) \end{array} \tag{2.21}$$

The parameter ϵ^* is the interaction energy, v^* is the characteristic volume of a lattice site, and r is the number of lattice sites occupied by a molecule of molecular weight M. T^*, P^*, ρ^* are derived from ϵ^*, v^* and r, as shown in equation 2.21. In application of the S-L EOS, T^*, P^*, ρ^* are often determined directly as the pure components parameters by an optimization procedure using PVT data.

The EOS for the mixture is formally identical to that of a pure component. However, "combining rules" are invoked to describe the interaction energy between unlike mers and the close-packed volume per mer. The com-

bining rules used in this work are given below:

$$\epsilon_{12}^* = \zeta \left(\epsilon_{11}^* \epsilon_{22}^*\right)^{1/2} \tag{2.22}$$

$$v^* = \phi_1 v_1^* + \phi_2 v_2^* + \phi_1 \phi_2 \delta \left(v_1^* + v_2^*\right) \tag{2.23}$$

where, ϵ_{12}^* is the interaction energy between mers of types 1 and 2, v^* is the close-packed volume per mer of the mixture, ϕ_1 and ϕ_2 are the mer fractions of components 1 and 2, ζ and δ are dimensionless parameters which can be evaluated by using an enthalpy and volume of mixing or a critical solution temperature and its critical composition.

The other two S-L parameters can be calculated:

$$\epsilon^* = \left(\phi_1^2 v_1^* \epsilon_{11}^* + \phi_1 \phi_2 \left(v_1^* + v_2^*\right)(1+\delta)\,\zeta \left(\epsilon_{11}^* \epsilon_{22}^*\right)^{1/2} + \phi_2^2 v_2^* \epsilon_{22}^*\right) / v^* \tag{2.24}$$

$$r = \left(\phi_1 / r_1 + \phi_2 / r_2\right)^{-1} \tag{2.25}$$

The chemical potential for component 1 in a binary mixture is [4]:

$$\begin{aligned} \mu_1 / kT = {} & \ln \phi_1 + \left(1 - r_1/r_2\right)\phi_2 + r_1 \chi_{12} \phi_2^2 \\ & + r_1 \left\{ -\tilde{\rho}/\tilde{T}_1 + \tilde{P}_1 \tilde{v}/\tilde{T}_1 + \tilde{v}\left[(1-\tilde{\rho})\ln\left(1-\tilde{\rho}\right) + \left(\tilde{\rho}/r_1\right)\ln\tilde{\rho}\right]\right\} \end{aligned} \tag{2.26}$$

where

$$\chi_{12} = \tilde{\rho} X_{12} / kT + \left(\tilde{P}_1 \tilde{v} / \tilde{T}_1\right)\left(1 + \upsilon^{-1}\right)\delta \tag{2.27}$$

$$X_{12} = \left(P_1^* P_2^*\right)^{1/2} v_1^* \left(v_2^* / v^*\right)^2 \left\{a + b_{12}\delta + c_{12}\delta^2\right\} \tag{2.28}$$

$$a = (\tau/\upsilon)^{1/2} + (\upsilon/\tau)^{1/2} - \left(\upsilon^{1/2} + \upsilon^{-1/2}\right)\zeta \tag{2.29}$$

$$b_{12} = \left\{\phi_1 \left(2 + \upsilon\phi_1\right)\left(\tau^{1/2} - \zeta\right) - \phi_2^2 \left(\zeta - \tau^{-1/2}\right)\right\}\left(\upsilon^{1/2} + \upsilon^{-1/2}\right) \tag{2.30}$$

$$c_{12} = \phi_2 \left(\tau^{1/2} - \zeta\right)(1+\upsilon)\left(\upsilon^{1/2} + \upsilon^{-1/2}\right) \tag{2.31}$$

$$\tau = T_1^*/T_2^* \tag{2.32}$$

$$\upsilon = v_1^*/v_2^* \tag{2.33}$$

Exchanging subscripts in equation 2.26-2.33 will result in the chemical potential for component 2. Also notice that these equations simplify considerably for $\delta = 0$.

For two components, given ϵ^*, v^*, r, and the two mixing parameters ζ and δ, the LF chemical potential and equation of state can be used to calculate the phase diagram. For a miscible liquid-vapor system, the composition in the vapor phase and the vapor pressure can be calculated at any liquid composition. The compositions of the two liquid phases present in a phase-separated system can also be calculated at a given temperature and pressure. Such calculations are carried out by equating the chemical potentials of each component in the two phases.

2.3 Interfacial Tension Theory for Pure System

According to equation 2.14, the interfacial tension for pure system is:

$$\gamma = \int_{-\infty}^{\infty} \left[\Delta a + (1/2)\left(\frac{d\rho}{dx}\right)^2 \kappa\right] dx \tag{2.34}$$

After minimization the following equations are obtained

$$\gamma = 2\int_{\rho_g}^{\rho_l} \sqrt{(1/2)\kappa\Delta a}\, d\rho \tag{2.35}$$

$$\Delta a = (1/2)\kappa \left(\frac{d\rho}{dx}\right)^2 \tag{2.36}$$

where ρ_g, ρ_l are the homogenous gas and liquid densities. Equation 2.35 can be conveniently rewritten in dimensionless form

$$\tilde{\gamma} = 2\int_{\tilde{\rho}_g}^{\tilde{\rho}_l} \sqrt{\tilde{\kappa}\Delta\tilde{a}}d\tilde{\rho} \tag{2.37}$$

$$\begin{array}{ll} \tilde{\gamma} = \gamma/\gamma^* & \gamma^* = \epsilon^*/v^{*2/3} \\ \kappa = 2\tilde{\kappa}\epsilon^* v^{*5/3} & \Delta\tilde{a} = \Delta a v^*/\epsilon^* \end{array} \tag{2.38}$$

$$\Delta\tilde{a} = \tilde{a}_0 - \tilde{a}_e = \tilde{P}_e - \tilde{\rho}^2 + \tilde{T}\left[(1-\tilde{\rho})\ln(1-\tilde{\rho}) + (\tilde{\rho}/r)\ln\tilde{\rho}\right] - \tilde{\rho}\tilde{\mu}_e \tag{2.39}$$

$$\tilde{\mu} = \mu/\left(r\epsilon^*\right) = -\tilde{\rho} + \tilde{P}\tilde{v} + \tilde{T}\left[(\tilde{v}-1)\ln(1-\tilde{\rho}) + (1/r)\ln\tilde{\rho}\right] \tag{2.40}$$

where $\tilde{a}_e$ is the reduced Helmholtz free energy of a two-phase equilibrium mixture of a two-phase equilibrium mixture of density ρ, $\tilde{\mu}_e$ is the reduced equilibrium chemical potential of the homogenous phase, and $\tilde{P}_e$ is the equilibrium vapor pressure.

2.4 Interfacial Tension Theory for Binary Mixtures

For a binary mixture, the governing equations for the interface may be written

$$\gamma = \int_{-\infty}^{\infty} \left[\Delta a + (1/2)\left(\kappa_{11}\rho_1'^2 + 2\kappa_{12}\rho_1'\rho_2' + \kappa_{22}\rho_2'^2\right)\right] dx \tag{2.41}$$

subject to

$$\begin{array}{l} \dfrac{\partial\Delta a}{\partial\rho_1} - \kappa_{11}\rho_1'^2 - \kappa_{12}\rho_2'^2 = 0 \\ \dfrac{\partial\Delta a}{\partial\rho_2} - \kappa_{12}\rho_1'^2 - \kappa_{22}\rho_1'^2 = 0 \end{array} \tag{2.42}$$

where the following simplified notation has been introduced:

$$\kappa_{ij} = \kappa_2^{ij} \tag{2.43}$$

$$\rho_i^{'} = \frac{d\rho_i}{dx} \tag{2.44}$$

We will use an inverse power law for the attractive part of the mer-mer interaction potential

$$\begin{array}{ll} u_{ij}(s) = \infty & s < \sigma_{ij} \\ u_{ij}(s) = -\epsilon_0^{ij} (\sigma_{ij}/s)^m & s \geq \sigma_{ij} \end{array} \tag{2.45}$$

In general, the exponent m depends on the i, j interaction so that from equation 2.9, we obtain

$$\kappa_{ij} = 2\epsilon_{ij}^* \sigma_{ij} \tilde{\kappa}_{ij} \tag{2.46}$$

where

$$\epsilon_{ij}^* = 2\pi\epsilon_0^{ij} / (m_{ij} - 3) \tag{2.47}$$

$$\tilde{\kappa}_{ij} = [(m_{ij} - 3) / (m_{ij} - 5)] / 6 \tag{2.48}$$

Making the substitution $\sigma_{ii}^3 = v_i^*$, the cross term κ_{12} can be evaluated by using the combining rules

$$\kappa_{12} = 2\zeta (\varepsilon_{11}^* \varepsilon_{22}^*)^{1/2} [(1/2)(v_1^* + v_2^*)(1 + \delta)]^{5/3} \tilde{\kappa}_{12} \tag{2.49}$$

Alternately, κ_{12} can be treated as an adjustable parameter. A useful simplification in the Euler equations can be achieved if κ_{12} is assumed to be given by

$$\kappa_{12} = (\kappa_{11}\kappa_{22})^{1/2} \tag{2.50}$$

Equation 2.42 then reduces to the algebraic form

$$\frac{1}{\kappa_{11}}\frac{\partial \Delta a}{\partial \rho_1} = \frac{1}{\kappa_{22}}\frac{\partial \Delta a}{\partial \rho_2} \tag{2.51}$$

For convenience in the discussion which follows, we define the dimensionless parameter

$$\omega = \kappa_{12} / \left(\kappa_{11}\kappa_{22}\right)^{1/2} \tag{2.52}$$

which expresses the deviation of κ_{12} from the geometric mean approximation. $\omega = 1$ represents the upper limit of permissible values for κ_{12}. This can be seen by examining equation 2.18 for a binary mixture

$$\Delta a = (1/2)\left(\kappa_{11}\rho_1^{'2} + 2\kappa_{12}\rho_1'\rho_2' + \kappa_{22}\rho_2^{'2}\right) \tag{2.53}$$

Clearly, if γ is to be positive, Δa must be positive, so that the quadratic form on the right-hand side of equation 2.53 must be positive definite. Since the x derivatives of ρ_1 and ρ_2 can be either positive or negative, $\omega < \kappa_{12} / \left(\kappa_{11}\kappa_{22}\right)^{1/2}$ or equivalently $\omega < 1$ is a necessary condition if the quadratic form is to be positive definite.

Numerical and analytical analysis is facilitated by transforming the equations from x space to ρ space. Such a transformation changes the limits of the integral in equation 2.41 from infinite to finite. Equation 2.53 can be rewritten as

$$\rho_1' = \pm\left[\frac{2\Delta a}{\kappa_{11} + 2\kappa_{12}\left(d\rho_2/d\rho_1\right) + \kappa_{22}\left(d\rho_2/d\rho_1\right)^2}\right]^{1/2} \tag{2.54}$$

Using this result to effect a change of variables in equation 2.41 yields

$$\gamma = 2^{1/2}\int_{\rho_1^{\mathrm{I}}}^{\rho_i^{\mathrm{II}}}\left[\kappa_{11} + 2\kappa_{12}\left(\frac{d\rho_2}{d\rho_1}\right) + \kappa_{22}\left(\frac{d\rho_2}{d\rho_1}\right)^2\right]\Delta a^{1/2} d\rho_1 \tag{2.55}$$

where I and II refer to the two equilibrium phases. Equation 2.54 can also be formally integrated to yield the interfacial tension profile

$$x - x_0 = \int_{\rho_1(x_0)}^{\rho_1(x)} \left[\kappa_{11} + 2\kappa_{12} \left(\frac{d\rho_2}{d\rho_1} \right) + \kappa_{22} \left(\frac{d\rho_2}{d\rho_1} \right)^2 \right] \Delta a^{-1/2} d\rho_1 \tag{2.56}$$

When the geometric mean approximation is used for κ_{12}, equation 2.51 is the minimization condition for equation 2.55. If κ_{12} is not equal to the geometric mean, equation 2.42 must be used, which reduces in ρ space to

$$\begin{aligned} &\left[\frac{\partial \Delta a}{\partial \rho_2} \left(\kappa_{11} + \kappa_{12} \frac{d\rho_2}{d\rho_1} \right) - \frac{\partial \Delta a}{\partial \rho_1} \left(\kappa_{12} + \kappa_{22} \frac{d\rho_2}{d\rho_1} \right) \right] \\ &\left[\kappa_{11} + 2\kappa_{12} \left(\frac{d\rho_2}{d\rho_1} \right) + \kappa_{22} \left(\frac{d\rho_2}{d\rho_1} \right)^2 \right] - 2\Delta a \left(\kappa_{11}\kappa_{22} - \kappa_{12}^2 \right) \frac{d^2\rho_2}{d\rho_1^2} = 0 \end{aligned} \tag{2.57}$$

Although the equations lose their symmetry and look much more complicated in ρ space, a great deal of computational simplicity is gained from this transformation.

Another simplification which applies only in the case where κ_{12} is assumed to follow the geometric mean has been employed in some cases. If one defines a variable

$$\Phi = \kappa_{11}^{1/2} \rho_1 + \kappa_{22}^{1/2} \rho_1 \tag{2.58}$$

the interfacial tension relationship may be written

$$\gamma = 2^{1/2} \int_{\Phi^{\mathrm{I}}}^{\Phi^{\mathrm{II}}} \Delta a^{1/2} d\Phi \tag{2.59}$$

and solved subject to equation 2.51. Care must be exercised in the use of this transformation, since integrating over Φ from Φ^{I} (i.e., Φ evaluated at ρ_1^{I} and ρ_2^{I} to Φ^{II} implies that Φ is monotonic. While this is usually true for well-behaved

low molecular weight mixtures, there is no guarantee that a smooth profile will result when this assumption is used. The profiles must thus always be monitored simultaneously as a check on such a calculation. Poser [5] discussed the numerical techniques employed to solve the interfacial problem for a binary mixture in the various approximations.

For the LF theory, the number density of mers, ρ_i, is identified as

$$\rho_i = \phi_i \tilde{\rho} / v^* \tag{2.60}$$

Using this definition along with equation 2.15, we obtain for the general combining rules

$$\begin{aligned} \Delta a = \varepsilon^* \tilde{\rho} / v^* \left\{ -\tilde{\rho} + \tilde{T} \left[(\tilde{v} - 1) \ln(1 - \tilde{\rho}) + \frac{1}{r} \ln \tilde{\rho} + \frac{\phi_1}{r_1} \ln \phi_1 + \frac{\phi_2}{r_2} \ln \phi_2 \right] \right\} \\ - \tilde{\rho} \phi_1 \mu_1^e / v^* - \tilde{\rho} \phi_2 \mu_2^e / v^* + P_e \end{aligned} \tag{2.61}$$

The μ_i^e must be given in units of energy/mer. Equations 2.41 and 2.42 can thus be solved by several methods of varying complexity. For liquid-vapor systems, results obtained with $\omega = 1$ are found to differ little from those calculated with $\omega < 1$. For liquid-liquid systems, on the other hand, the results are very sensitive to the value of ω.

2.5 Bibliography

[1] Cahn, J. W.; Hilliard, J. E. *Journal of Chemical Physics* **1958**, *28*, 258–67.

[2] Bongiorno, V.; Davis, H. T. *Physical Review A* **1975**, *12*(5), 2213–2224.

[3] Sanchez, I. C.; Lacombe, R. H. *Journal of Physical Chemistry* **1976**, *80*(21), 2352–2362.

[4] Sanchez, I. C. *Journal of Macromolecular Science-Physics* **1980**, *B17*(3), 565–589.

[5] Poser, C. I. Ph. d. thesis, University of Massachusetts, **1980**.

Chapter 3

Adsorption on Polymer Surfaces

Recent studies [1] of CO_2 sorption onto polymer thin films supported on the inorganic substrates have shown interesting anomalous behavior near the CO_2 critical point. As the bulk CO_2 approaches the critical point, the thin polymer film appears to thicken. The mechanism of the film thickening is unclear: it may be that the CO_2 is forming a liquid layer on the surface of the polymer film, or the CO_2 is absorbing into the film and swelling it. A combination of the gradient theory of inhomogeneous systems and Sanchez-Lacombe equation of state has been used to investigate this phenomenon. Understanding of the interaction between supercritical fluids and polymer films will give pathways for developing applications; include polymer welding, polymer synthesis, chemical extraction, semiconductor manufacture and industrial cleaning.

The free energy approach to the theoretical description of interfaces between fluid phases has a long and active history starting from van der Waals [2]. Bongiorno and Davis [3] derived their interfacial theory by combing the gradient theory [4] with the van der Waals's equation of state, and obtained

[1]Reprinted with permission from Wang X. and Sanchez, I.C. *Langmuir* **2006**, 22(22), 9251-9253. Copyright ©2006 American Chemical Society

reasonable results for simple fluids. Poser and Sanchez [5] extended the interfacial calculation to include polymer liquids by incorporating the Sanchez-Lacombe equation of state [6].

This paper theoretically investigates critical adsorption on an attractive wall, numerical methods are also presented for the adsorption of CO_2 on polymer thin films PDMS (polydimethyl siloxane) [7] PIB [8] and (1,1-difluoroethane) [9] on PS (polystyrene) thin film. By calculating the Gibbs adsorption and adsorption layer thickness of the supercritical fluids, we found in all cases (different substrates, different supercritical fluids) that maximum adsorption occurs when the supercritical fluid is near its compressibility maximum.

3.1 CO_2 with Attractive Wall

Critical adsorption of CO_2 with an attractive wall is a relatively simple case for analysis, but it will shed light on the physics of critical adsorption.

3.1.1 Properties of CO_2

Experimentally, supercritical CO_2 has a readily accessible critical temperature (T_c) of 30.97 °C and a critical pressure (P_c) of 7.38 MPa. but critical parameters calculated from S-L EOS using the lattice fluid parameters in Table 3.1 are a little different (T_c: 31.63 °C, P_c: 8.91 MPa).

The special characteristic of supercritical fluid is large density fluctuations in the system. Figure 3.1 show the dimensionless compressibility of

Table 3.1: Lattice Fluid Parameters

	T^* (K)	P^* (MPa)	ρ^* (kg/m^3)	T_g (°C)	r
CO_2	283	659	1620		7.6
1,1-difluoroethane	402	366.4	1206		6.0
PDMS	476	302	1104	-125 [10]	
PS	735	358	1105	90	
PIB	643	354	974	-71.2 [11]	

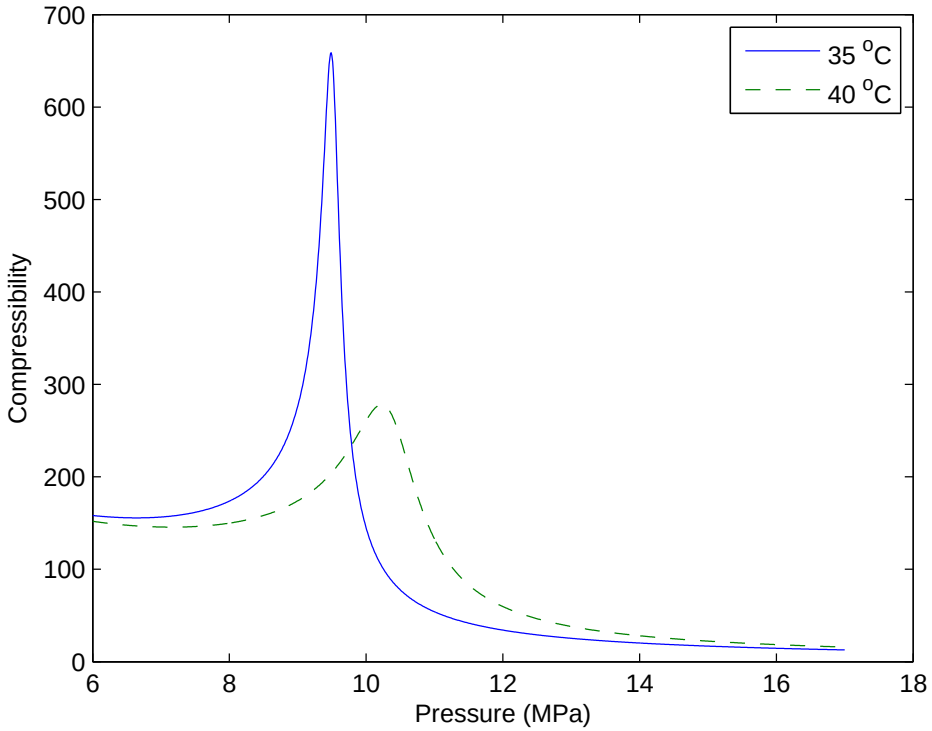

Figure 3.1: Compressibility *vs.* Pressure of CO_2

CO_2 under the isothermal condition near the critical point. The dimensionless compressibility is defined as:

$$P^*\beta = P^*\frac{\partial \ln \rho}{\partial P} = \frac{\tilde{v}^2}{\tilde{T}\tilde{v}[1/(\tilde{v}-1)+1/r]-2} \tag{3.1}$$

From this figure, we can see that the characteristic features of density fluctuation in the supercritical region are (1) there is a peak in each lateral curve, (2) the amplitude of the fluctuation diverges as the critical point is approached, and (3) the width of the peak broadens with increasing temperature. And the locus of the peaks in the compressibility forms the ridge of density fluctuations. Some experiments [1, 12] showed that anomalous sorption on the density fluctuation ridge, and we will try to understand the relationship between the critical sorption and density fluctuation.

3.1.2 Analytical Analysis

Consider the free energy of the semi-infinite fluid in contact with a planar attractive wall at x=0. Let us assume that the surface is solid and sharp on an atomic scale and that the interactions between surface and fluid are sufficiently short-range that the contribution to the free energy of a unit area of this surface is $\Phi(\rho_s)$ [13], where ρ_s is the limiting fluid density at x=0. We further assume $\Phi(\rho_s)$ is linearly dependent on ρ_s.

$$\gamma = \Phi\left(\rho_s\right) + \int_0^\infty \left[\Delta a + \frac{1}{2}\kappa\left(\frac{d\rho}{dx}\right)^2\right] dx \tag{3.2}$$

$$\phi = -\left.\frac{d\Phi}{d\rho_s}\right|_{x=0} \tag{3.3}$$

where ϕ is a positive constant.

By definition, the Gibbs adsorption Γ can be calculated from the equation

$$\Gamma(P) = \int_0^\infty (\rho - \rho_e)\, dx \tag{3.4}$$

Numerical and analytical analysis is facilitated by transforming the equation from x space to ρ space; using equation 2.36 to effect a change of variable yields

$$\Gamma(P) = \int_0^\infty (\rho - \rho_e)\, dx = \int_{\rho_e}^{\rho_s} \frac{\sqrt{\kappa}\,(\rho - \rho_e)}{\sqrt{2\Delta a}} d\rho \tag{3.5}$$

where ρ_s is determined from the natural boundary condition at x=0

$$\phi = -\kappa \left(d\rho/dx\right)|_{x=0} = \sqrt{2\kappa\Delta a\,(\rho_s)} \tag{3.6}$$

To make progress, Δa must be evaluated; expanding Δa in a series around the liquid density yields

$$\Delta a = \frac{1}{2}\frac{(\rho - \rho_e)^2}{\rho_e^2 \beta} + \cdots \tag{3.7}$$

Substitute of equation 3.7 into boundary condition equation 3.6 and subsequent simple arithmetic yields

$$\rho_s - \rho_e = \phi\sqrt{\frac{\beta}{\kappa}}\rho_e \tag{3.8}$$

From equation 3.7 and equation 3.9, it follows that

$$\Gamma(P) = \int_{\rho_e}^{\rho_s} \frac{\sqrt{\kappa}\,(\rho - \rho_e)}{\sqrt{2\Delta a}} d\rho \approx \sqrt{\kappa\beta}\rho_e\,(\rho_s - \rho_e) \approx \phi\beta\rho_e^2 \tag{3.9}$$

From above analysis, we found that when the free energy approximation is valid (ϕ is small), the maximum of Gibbs adsorption excess occurred at a pressure where $\beta\rho^2$ reached its maximum, instead of a pressure where β reached its maximum.

3.1.3 Numerical Analysis

The validity of the free energy approximation 3.7 depends on the deviation of fluid density from equilibrium density, and the deviation becomes bigger when ϕ is bigger. Numerical methods should be used if we don't take this approximation. Equation 3.5 and equation 3.6 can be conveniently rewritten in dimensionless form

$$\tilde{\Gamma}\left(\tilde{P}\right) = \frac{\Gamma}{\rho^* v^{*1/3}} = \int_0^\infty \left(\tilde{\rho} - \tilde{\rho}_e\right) d\tilde{x} = \int_{\tilde{\rho}_e}^{\tilde{\rho}_s} \frac{\sqrt{\tilde{\kappa}}\left(\tilde{\rho} - \tilde{\rho}_e\right)}{\sqrt{\Delta\tilde{a}}} d\tilde{\rho} \tag{3.10}$$

$$\tilde{\phi} = \frac{\phi}{\epsilon^* v^{*1/3}} = 2\sqrt{\tilde{\kappa}\Delta\tilde{a}\left(\tilde{\rho}_s\right)} \tag{3.11}$$

where $\tilde{a}_e$ is the reduced Helmholtz free energy of a two-phase equilibrium mixture of a two-phase equilibrium mixture of density ρ, $\tilde{\mu}_e$ is the reduced equilibrium chemical potential of the homogenous phase, and $\tilde{P}_e$ is the equilibrium vapor pressure.

In [14], a constant value of $\tilde{\kappa} = 0.62$ was found to reproduce the interfacial tensions of a wide range of nonpolar and slightly polar low molecular weight liquids over a large temperature interval with an error of about 5 %. Here we use this value of $\tilde{\kappa}$ and set $\tilde{\phi}$ as 0.01 to perform the calculation of calculation of $\tilde{\Gamma}\left(\tilde{P}\right)$, and the increment of P is set to 0.01 MPa. Figure 3.2

illustrates the calculated values of $\tilde{\Gamma}$ as a function of P, and the adsorption has a maximum with increasing pressure. To compare the locus of this maximum and those of $\beta\rho^2$ and β, we plot these values in normalized form in the same figure (See Figure 3.3). In Figure 3.4, the same quantities are compared with a bigger $\tilde{\phi}$ (0.2). From these two figures, we can see that (1) the locus of maximum of $\beta\rho^2$ and β are almost the same, (2) when $\tilde{\phi}$ is small (0.01), the locus of maximum of Gibbs adsorption is close to that of $\beta\rho^2$, and this agrees well with the conclusion of analytical analysis. When $\tilde{\phi}$ is bigger (0.2), the distance between the two loci becomes bigger, and it shows that the free energy approximation is not valid for this $\tilde{\phi}$ (0.2).

3.2 Polymer-Supercritical Fluid System

The analysis of equilibrium properties is the basis for calculation of surface properties. For binary systems of polymer-gas mixture, we can assume the volume fraction of polymer in the vapor phase is zero because it is very difficult for polymer to vaporize. So, the equilibrium can be find by equating the chemical potential of gas in two phases.

$$\mu_1^{\mathrm{I}}\,(\text{gas}) = \mu_1^{\mathrm{II}}\,(\text{gas absorbed in polymer}) \tag{3.12}$$

To perform equilibrium calculation, we need to first determine the binary interaction parameters, ζ and δ. The polymer-gas systems we considerer here included: Poly(dimethyl siloxane)/CO_2 [15], PIB (polyisobutylene)/CO_2 [8], Polystyrene (1,1-difluoroethane) [9]. The two parameters for the polymer-

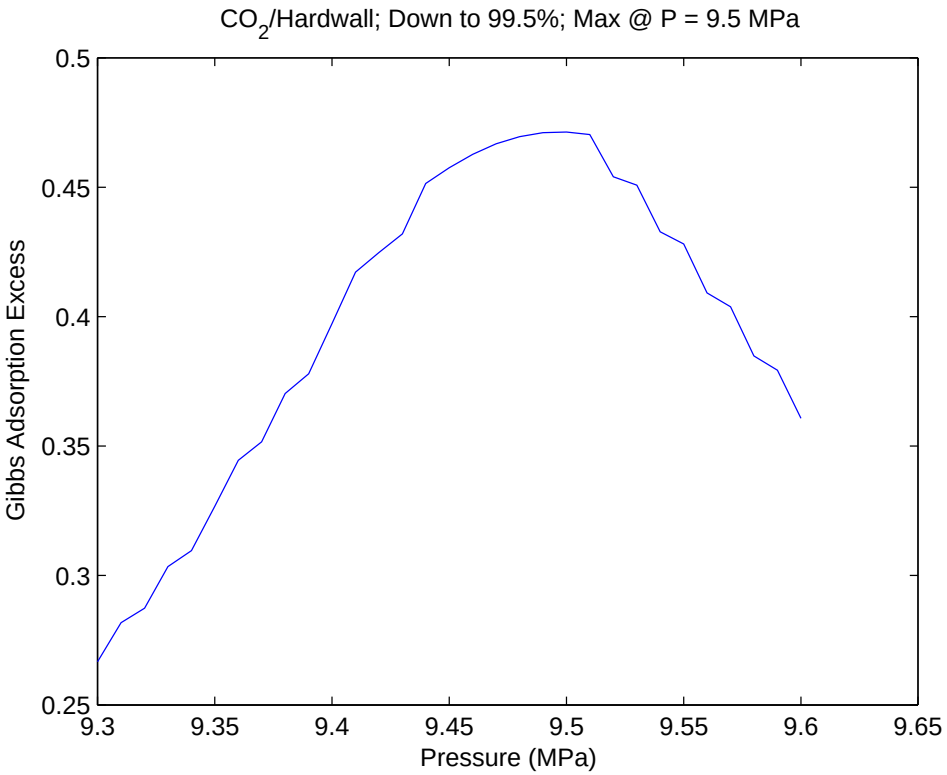

Figure 3.2: Gibbs Adsorption *vs.* Pressure of CO_2

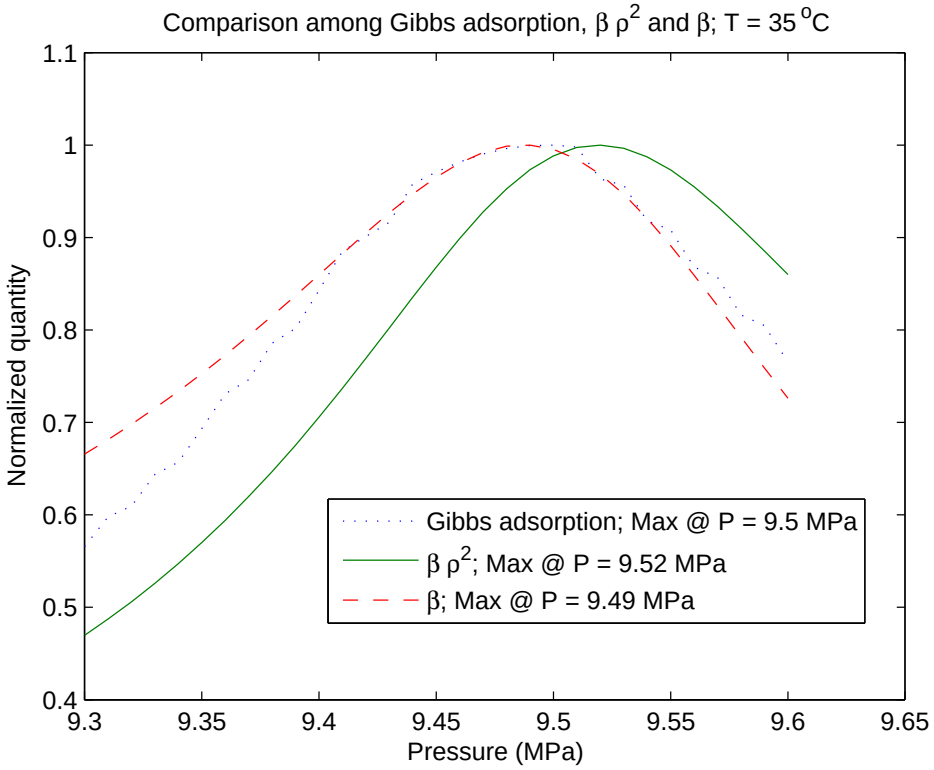

Figure 3.3: Comparison among Gibbs Adsorption, $\beta\rho^2$ and β of CO_2: $\tilde{\phi} = 0.01$

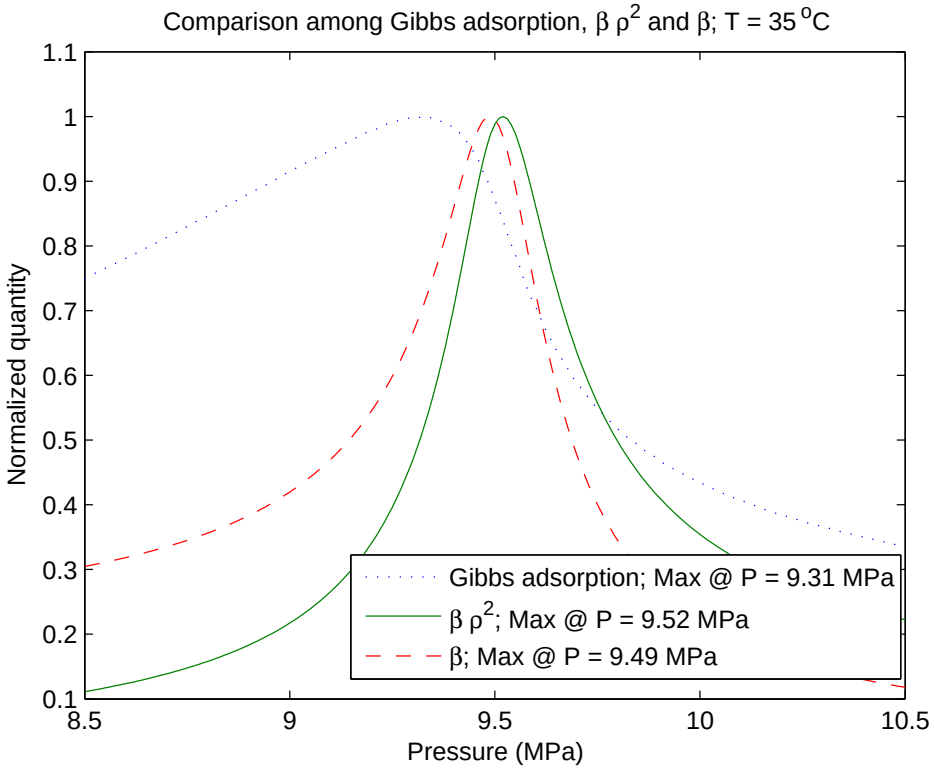

Figure 3.4: Comparison among Gibbs Adsorption, $\beta\rho^2$ and β of CO_2: $\tilde{\phi} = 0.2$

Table 3.2: Binary solvent/polymer interaction parameter

		ζ	δ	T (°C)
PDMS	CO_2	0.9512	0.0154	35
PIB	CO_2	0.8996	0.0266	35
PS	1,1-difluoroethane	0.940	0.062	135

gas systems can be obtained by fitting the experimental swelling data, just as listed in Table 3.2. The experimental swelling data were taken from the literature cited.

3.2.1 Properties of 1,1-difluoroethane

Experimentally, critical parameters for supercritical 1,1-difluoroethane are: critical temperature (T_c) 113.4 °C, critical pressure (P_c) 4.5 MPa. And critical parameters calculated from S-L EOS using the lattice fluid parameters in Table 3.1 are (T_c: 132.24 °C, P_c: 6.44 MPa). Figure 3.5 show the non-dimensional compressibility of 1,1-difluoroethane under the isothermal condition near the critical point.

3.2.2 Numerical Analysis

To calculate the surface properties, there are a few parameters should be determined. ω is chosen as 1 to make the calculation simple. $\tilde{\kappa}$ for small molecules (CO_2 and 1,1-difluoroethane) is set to 0.62, and that for polymers (PDMS, PIB and PS) is set to be 0.55.

Instead of Gibbs adsorption, here we calculate the thickness of the

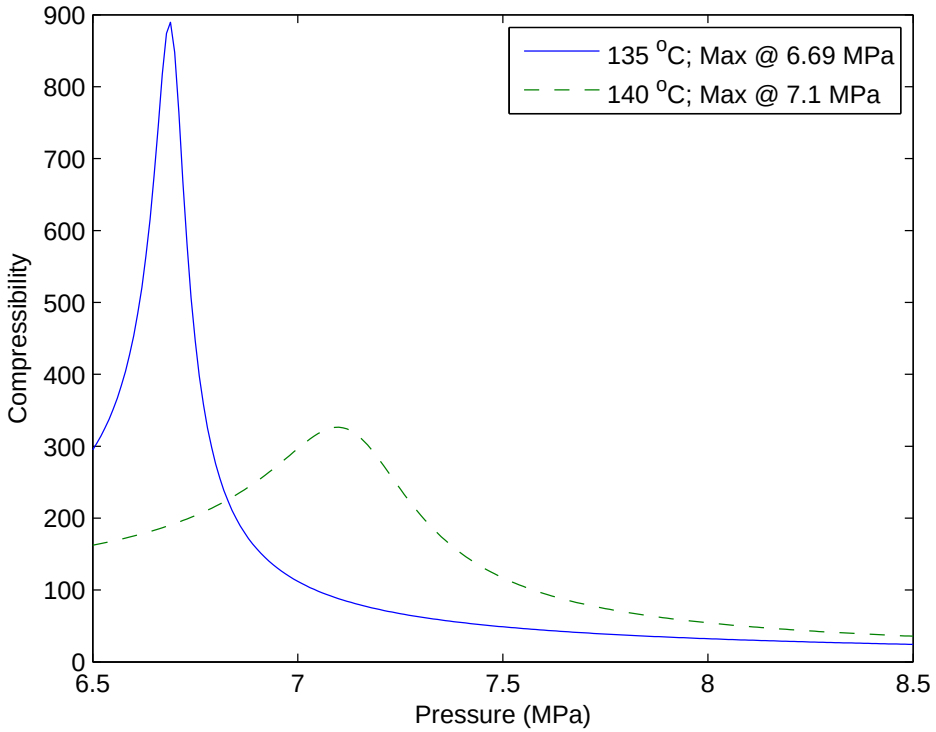

Figure 3.5: Compressibility *vs.* Pressure of 1,1-difluorethane

adsorbed layer. The thickness is defined as the distance from x=0 to where the mer density of the supercritical fluid drops to 10% of $(\rho_{\max} - \rho_{\mathrm{e}})$, just as shown in Figure 3.6 (the surface thickness is the thick line in the figure). Figure 3.7, Figure 3.8 and Figure 3.9 show the the thickness of adsorbed layer varies with the pressure for system PDMS/CO_2, PIB/CO_2 and PS/1,1-difluoroethane, respectively. From these figures, we found that supercritical fluids have a maximum adsorption near critical region. Comparing these figures with the compressively of CO_2 (Figure 3.1) and 1,1-difluoroethane (Figure 3.5), we find that the maximum adsorption occur on the density fluctuation ridge.

3.3 Conclusion

This paper theoretically investigates critical adsorption on an attractive wall. Numerical results are also presented for the adsorption of CO_2 on polymer thin films PDMS, PIB and supercritical 1,1-difluoroethane on PS thin film. By calculating the Gibbs adsorption and adsorption layer thickness of the supercritical fluids, we found in all cases (different substrates, different supercritical fluids) that maximum adsorption occurs when the supercritical fluid is near its compressibility maximum.

This conclusion is different than reached by Koga, et.al. [12, 16] from neutron reflectivity measurements. They concluded that near the compressibility maximum, supercritical fluid absorption is enhanced in thin films relative to thick films. However, their conclusion is based on the scattering model used to interpret the neutron reflectivity measurements. We believe that a re-

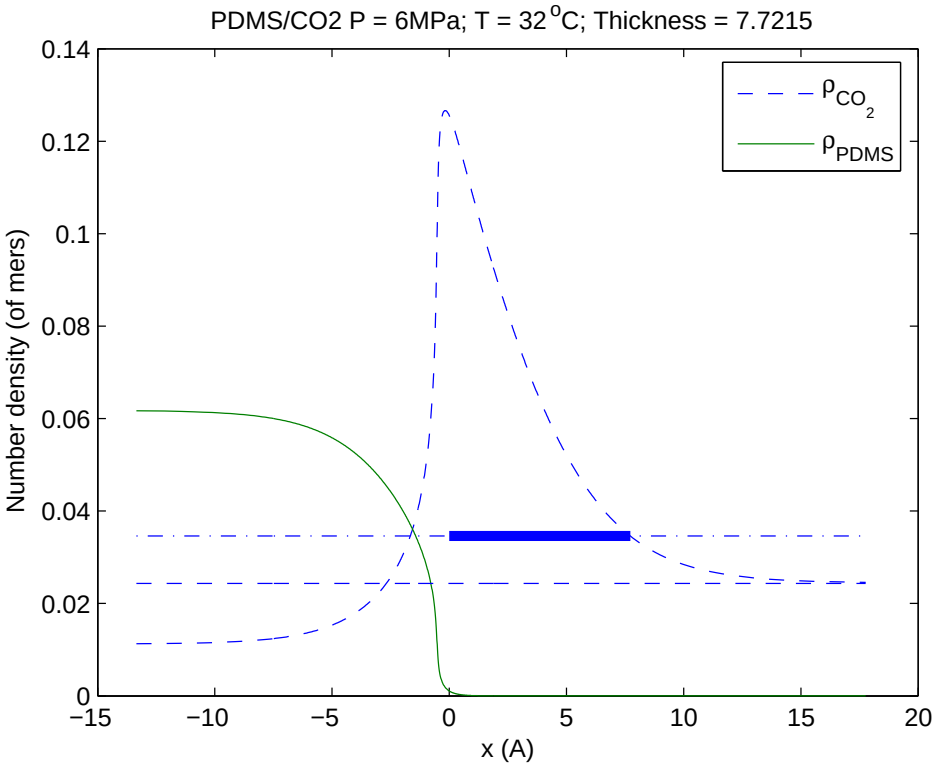

Figure 3.6: Definition of thickness of adsorbed layer

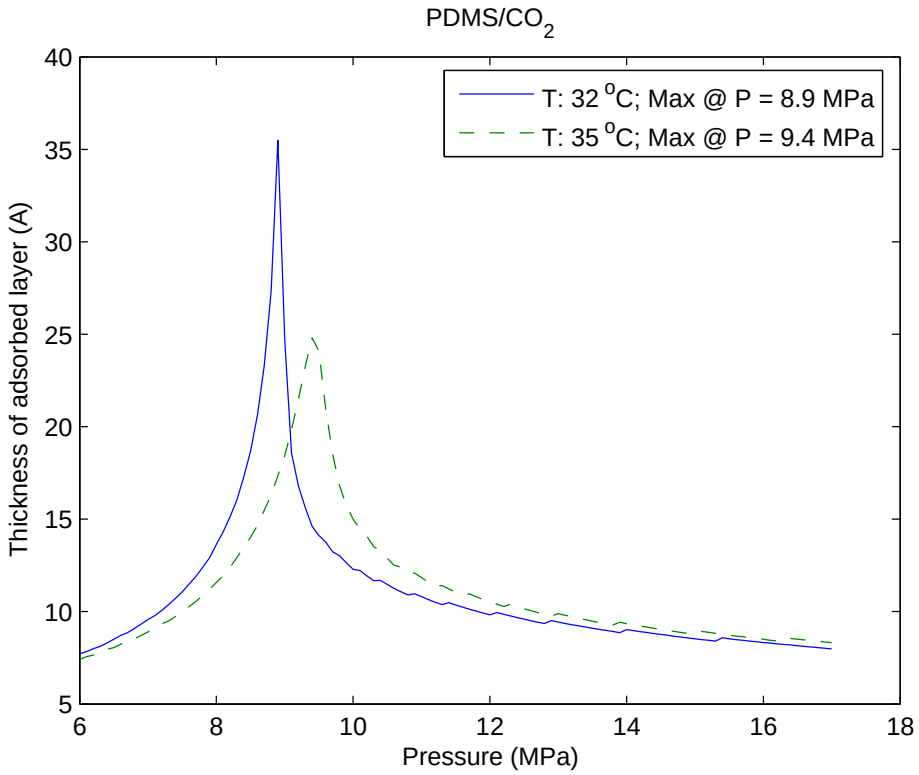

Figure 3.7: Thickness of adsorbed layer for PDMS/CO_2

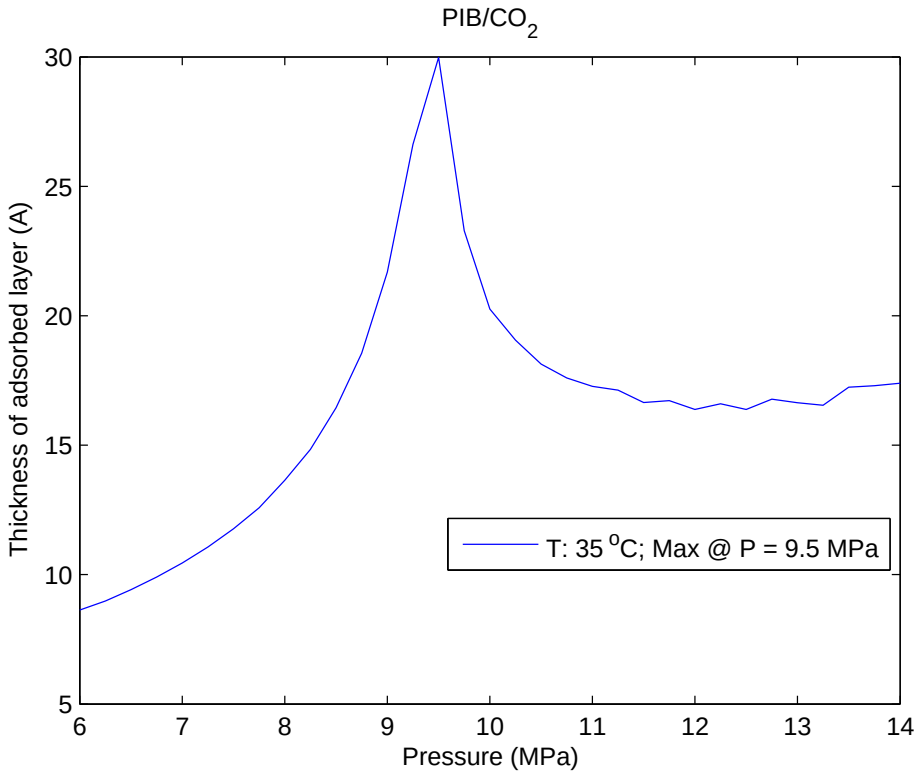

Figure 3.8: Thickness of adsorbed layer for PIB/CO_2

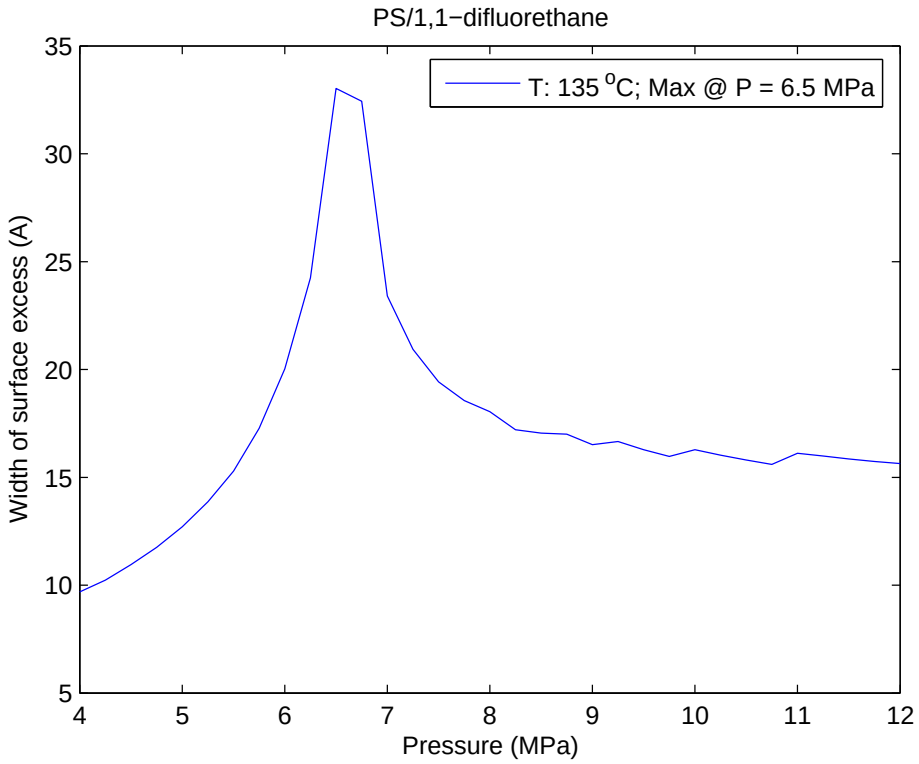

Figure 3.9: Thickness of adsorbed layer for PS/1,1-difluorethane

analysis of their data using an adsorbed layer model would also be compatible with our conclusion that the observed anomalous sorption is related to critical wetting.

3.4 Bibliography

[1] Sirard, S. M.; Ziegler, K. J.; Sanchez, I. C.; Green, P. F.; Johnston, K. P. *Macromolecules* **2002**, *35*(5), 1928–1935.

[2] Rowlinson, J. S. *Journal of Statistical Physics* **1979**, *20*(2), 197–244.

[3] Bongiorno, V.; Davis, H. T. *Physical Review A* **1975**, *12*(5), 2213–2224.

[4] Cahn, J. W.; Hilliard, J. E. *Journal of Chemical Physics* **1958**, *28*, 258–67.

[5] Poser, C. I.; Sanchez, I. C. *Macromolecules* **1981**, *14*(2), 361–70.

[6] Sanchez, I. C.; Lacombe, R. H. *Journal of Physical Chemistry* **1976**, *80*(21), 2352–2362.

[7] Pope, D. S.; Sanchez, I. C.; Koros, W. J.; Fleming, G. K. *Macromolecules* **1991**, *24*(8), 1779–1783.

[8] Chang, S. H.; Park, S. C.; Shim, J. J. *Journal of Supercritical Fluids* **1998**, *13*(1-3), 113–119.

[9] Garg, A.; Gulari, E.; Manke, C. W. *Macromolecules* **1994**, *27*(20), 5643–5653.

[10] Brandrup, J.; Immergut, E. H.; Grulke, E. A.; 4th ed., 1999.

[11] Mark, J. E.; 1 st ed., 1999.

[12] Koga, T.; Seo, Y. S.; Shin, K.; Zhang, Y.; Rafailovich, M. H.; Sokolov, J. C.; Chu, B.; Satija, S. K. *Macromolecules* **2003**, *36*(14), 5236–5243.

[13] Cahn, J. W. *Journal Of Chemical Physics* **1977**, *66*(8), 3667–3672.

[14] Poser, C. I.; Sanchez, I. C. *Journal of Colloid and Interface Science* **1979**, *69*(3), 539–548.

[15] Royer, J. R.; DeSimone, J. M.; Khan, S. A. *Macromolecules* **1999**, *32*(26), 8965–8973.

[16] Koga, T.; Seo, Y.-S.; Zhang, Y.; Shin, K.; Kusano, K.; Nishikawa, K.; Rafailovich, M. H.; Sokolov, J. C.; Chu, B.; Peiffer, D.; Occhiogrosso, R.; Satija, S. K. *Physical Review Letters* **2002**, *89*(12), 125506/1–125506/4.

Chapter 4

Polymer Welding

The effect of adding a solvent to a blend system depends on the amount of solvent. In dilute polymer solutions, it is possible for two polymers to dissolve in the solvent even if the two polymers are incompatible by their own. But we will not consider these solvent-rich systems, but rather systems where the solvent is the minor component.

Welding is defined as the process in which thermoplastics are united, fused, or brought into intimate contact. The materials are softened by heat or solvents, brought into contact, and held together under pressure until the weld cools or the solvent evaporates. Polymers can be welded by several techniques, including hot plate welding, hot air welding, vibrational welding, friction welding, solvent welding, dielectric welding, adhesive bonding, surface chemical modification, ion beam surface modification, resonance heating, and other more elaborate but less common techniques.

It is useful to briefly outline here the main theoretical and experimental results describing the structure and strength of polymer interfaces. At first, one should differentiate between two general types of interfaces: the case where the two polymers on either side of the interface are miscible, which

are sometimes called symmetric interfaces, when the identical polymers are on both sides, and the asymmetric case where the two polymer on either side of the interface are immiscible. Note that this definition has nothing to do with the symmetry of the interfacial concentration profile, which is symmetric in both cases; only in the case of strong difference of T_g, can the profile become asymmetric. In the first case, the problem is a kinetic one, where it is important to understand the dynamics of the diffusing chains across the plane of the interface, and the structure of the interface can be controlled with the annealing time and molecular weight of the polymers. In the second case, we are faced with a thermodynamics problem. Buxton built a model to predict the mechanical properties of binary blends of immiscible polymers [1]. Lattice spring model (LSM) was used to calculate the fracture energy of glassy polymer-polymer interfaces [2]. Schnell addressed the direct correlation between interfacial width and adhesion in glassy polymers [3].

Polymer adhesion between two immiscible polymers is usually poor because there is little interpenetration of one polymer into the other at the interface. Increasing the width of the interfacial zone can enhance adhesion and mechanical properties. In principle, this can be accomplished by exposing the solid polymer materials to a supercritical fluid. The supercritical fluid can act as a common solvent (It reduces the unfavorable interaction parameter by dilution) and promote interpenetration. It also increases chain mobility at the interface that helps to promote "welding" of the two polymers. The welding process can be carried out at elevated temperatures to facilitate in-

terpenetration kinetics. After exposing and swelling the polymers with CO_2 and increasing the interfacial zone, the system would be quickly depressurized and allowed to return to room temperature. The key here is that the system will not have enough time to return to its equilibrium condition. The new, thicker, and better adhering interface will be retained. This condition (kinetically stable interface) will remain for as long as the polymer use temperature is well below the glass temperature of either polymer.

A combination of the gradient theory of inhomogeneous systems and the Sanchez-Lacombe equation of state used to investigate this phenomenon, especially the effect of high compressibility of supercritical fluid to the compatibilization of two incompatible polymers. We calculate the interfacial density profile, interfacial thickness and interfacial tension between the two polymers with and without the supercritical fluid. We find that the interfacial tension is decreased and the interfacial thickness is increased with high pressure supercritical fluid for the ternary systems we have investigated. As the critical point is approached and the supercritical compressibility becomes large, no enhancement or deleterious effects on compatibilization were observed.

4.1 Introduction

Supercritical carbon dioxide is widely used as a regeneration solvent in a range of technical and chemical processes, such as chromatography, extraction, reactor cleanup, and preparation of pharmaceutical products [4]. Large changes in the density of supercritical fluid can be achieved with small vari-

ations in pressure and/or temperature, resulting in the ability to tune the density dependent solvent properties, such as dielectric constant, viscosity, and diffusivity.

Blending of immiscible polymers offers scientists and technologists an opportunity to create materials with improved properties, such as impact strength, rigidity etc., compared with the individual polymers. Supercritical CO_2 has been used to assist the preparation of polymer blends by batch mixing and extrusion [5]. The greater reduction in viscosity of the minor component with the addition of CO_2 allows better momentum transfer from the more viscous major component. This leads to a finer dispersion of the minor component and improved mechanical properties. High-power batch mixers and twin screw extruders are the most commonly used apparatuses for this processing.

Helfand [6–8] developed a theory of interfacial tension between polymer pairs of infinite molecular weight. Hong and Noolandi [9, 10] generalized the Helfand theory and used scaling arguments to describe the effect of solvent on the interfacial properties of two incompatible polymers.

In order to investigate whether highly compressibility supercritical fluids have an effect on compatibilization, a combination of the gradient theory of inhomogeneous systems and Sanchez-Lacombe equation of state has been used to investigate this phenomenon. Understanding of the interaction between supercritical fluids and polymer films will give pathways for developing applications that include polymer welding, polymer synthesis, chemical ex-

traction, semiconductor manufacture and industrial cleaning.

The free energy approach to the theoretical description of interfaces between fluid phases has a long and active history starting with van der Waals [11]. Bongiorno and Davis [12] derived their interfacial theory by combining the gradient theory [13] with the van der Waals's equation of state, and obtained reasonable results for simple fluids. Poser and Sanchez [14] extended the interfacial calculation to include polymer liquids by incorporating the Sanchez-Lacombe equation of state [15] and this method has been used to investigated the anomalous sorption of supercritical fluid into polymer thin films [16].

This paper extends the interfacial theory for binary system [14] to n-component system and numerically investigates the interfacial tension and interfacial thickness with and without supercritical fluids. The systems investigated include: PIB(polyisobutylene)/PDMS(poly dimethyl siloxane)/CO_2, PnBMA(poly n-butyl methacrylate)/PDMS/CO_2 and PnBMA/PDMS/C_2H_6. By comparing the change of the interfacial thickness with and without supercritical fluid, we found that the interfacial thickness is increased and interfacial tension is decreased with the high pressure supercritical fluid in these systems.

We would be remiss not to mention that the general scenario outlined above may not be universal. An apparent exception can be found in blends of PDMS/PEMS (polyethylmethylsiloxane) [17]. The upper critical solution temperature (UCST) of this blend increases with increasing CO_2 pressure. This implies that the supercritical fluid increases the interfacial tension in contrast to what intuition suggests and what we have found. Theoretically, it

occurs when:

$$|\chi_{AS} - \chi_{BS} + (N_A - N_B)/2N_AN_B| > N_A^{-1/2} + N_B^{-1/2} \tag{4.1}$$

Where χ_{AS}, χ_{BS} are the polymer solvent interaction parameters; N_A, N_B are the degrees of polymerization. In general, an increase in interfacial tension will be observed whenever the solvent is preferentially rejected from the interface.

4.2 Interfacial Theory for n-component System

Poser and Sanchez [18] formulated how to calculate the interfacial tension and interfacial for binary system. The extension to ternary system is quite straight forward based on the simplicity and structure of the formulation.

For a n-component system, we assume two bulk phases are on each side of the interface, the equilibrium density of the components in phase I is ρ_i^I, and ρ_i^{II} in phase II. The governing equations for the interface may be written

$$\gamma = \int_{-\infty}^{\infty} \left[\Delta a + (1/2) \sum_i \sum_j \kappa_{ij} \left(d\rho_i/dx\right) \left(d\rho_j/dx\right) \right] dx \tag{4.2}$$

subject to

$$\frac{\partial \Delta a}{\partial \rho_i} - \kappa_{i1} \frac{d^2\rho_1}{dx^2} - \kappa_{i2} \frac{d^2\rho_2}{dx^2} - \cdots - \kappa_{in} \frac{d^2\rho_n}{dx^2} = 0 \, (i = 1, 2, \cdots, n) \tag{4.3}$$

where γ is interfacial tension, Δa is the excess Helmholtz free energy in the absence of interfacial density gradient, ρ is the fluid density at position x, $1/2\kappa_{ij} \left(d\rho_i/dx\right) \left(d\rho_j/dx\right)$ is the free energy contribution from the interfacial density gradient, κ_{ij} scales the contribution of the quadratic gradient term and is a positive constant.

A useful simplification in the Euler equations can be achieved when κ_{ij} is assumed to be given by

$$\kappa_{ij}^{*} = \left(\kappa_{ii}^{*}\kappa_{jj}^{*}\right)^{1/2} \tag{4.4}$$

If κ_{ij} is assumed to follow the geometric mean, equation 4.3 then reduced to the algebraic form

$$\frac{1}{\sqrt{\kappa_{11}}}\frac{\partial \Delta a}{\partial \rho_1} = \frac{1}{\sqrt{\kappa_{22}}}\frac{\partial \Delta a}{\partial \rho_2} = \cdots = \frac{1}{\sqrt{\kappa_{nn}}}\frac{\partial \Delta a}{\partial \rho_n} \tag{4.5}$$

Defining a variable

$$\Phi = \sum_i \kappa_{ii}\rho_i^{1/2} \tag{4.6}$$

and using the geometric mean for κ_{ij}, the interfacial tension and interfacial profile can be written as

$$\gamma = 2\int_{\Phi^{\mathrm{I}}}^{\Phi^{\mathrm{II}}} \sqrt{\Delta a}\, d\Phi \tag{4.7}$$

$$x - x_0 = \int_{\Phi_0}^{\Phi} \sqrt{\frac{1}{\Delta a}}\, d\Phi \tag{4.8}$$

These equations can be solved subject to equation 4.5 where Φ^{I} is Φ evaluated at ρ_i^{I} and Φ^{II} is Φ evaluated at ρ_i^{II}.

4.3 Application to Polymer Blend and Solvent Systems

The ternary systems we have studied are composed of polymer blends and a supercritical fluid. The systems considered in this paper include: PIB/PDMS/CO_2, PnBMA/PDMS/CO_2 and PnBMA/PDMS/C_2H_6. The interfacial tension and interfacial thickness have been calculated between the polymers with and without the high pressure supercritical fluid. To perform these calculations,

we need to determine the binary interaction parameters defined in Sanchez-Lacombe model (ζ and δ) between each of two components in the ternary systems listed above. The parameters between polymer and solvent can be obtained by a non-linear least square fit of experimental swelling data; the parameters are listed in Table 4.1. The experimental swelling data were taken from the literature listed in Table 4.1. Polymer-polymer interaction parameters are difficult to measure experimentally and reliable data are scarce. We set ζ for polymer-polymer interaction to be 0.99 and ζ for polymer-polymer interaction to be -0.0025. These values guarantee that the polymer pairs will be immiscible.

Experimentally, CO_2 has a critical temperature (T_c) of 31.0 °C and a critical pressure (P_c) of 7.38 MPa, but the critical parameters calculated from the Sanchez-Lacombe EOS are a little different. (T_c: 31.63 °C, P_c: 8.91 MPa). For C_2H_6, experimental T_c is 29.65 °C and P_c is 2.98 MPa, calculated T_c is 30.48 °C and P_c is 5.66 MPa. The compressibility and the adsorption of the fluid is dependent on how far the working condition is from the critical point; the critical parameters calculated from the equation of state are more important than the experimental critical parameters in this study.

To calculate the interfacial properties, there are two more parameters (ω_{ij} [$=\kappa_{ij}/\left(\kappa_{ii}\kappa_{jj}\right)^{1/2}$] and $\tilde{\kappa}_{ii}$) to be determined. ω_{ij} expresses the deviation of κ_{ij} from the geometric mean approximation, and $\tilde{\kappa}_{ii}$ is the dimensionless form of κ_{ii} ($\kappa_{ii} = \tilde{\kappa}_{ii}\varepsilon_i^* v_i^{*5/3}$), where ε_i^* and v_i^* parameters defined in the Sanchez-Lacombe EOS). ω_{ij} is chosen as 1 to make the calculation simple. $\tilde{\kappa}_{ii}$ for small

molecules (CO_2 and C_2H_6) is set to 0.62, and that for polymers (PDMS, PIB and PnBMA) is set to be 0.55 [18].

Figure 4.1 shows the interfacial density profile of PIB/PDMS/CO_2. In the interfacial region, the first component PIB is monotonically decreasing from PIB rich PDMS poor side to the other; but the second component PDMS is not; there is a local maximum density ($\rho^{\max}_{\mathrm{PDMS}}$) in the interfacial region. The interfacial thickness is operationally defined as the distance between x_{A} and x_{B} (as shown in Figure 4.1). x_{A} is the position where the local density of the first component PIB is 90% of the bulk density of PIB on PIB rich-PDMS poor side ($\rho^{\mathrm{bulk}}_{\mathrm{PDMS}}$). x_{B} is the position where the local density of the second component PDMS is equal to $\rho^{\max}_{\mathrm{PDMS}} - 90\%(\rho^{\max}_{\mathrm{PDMS}} - \rho^{\mathrm{bulk}}_{\mathrm{PDMS}})$; $\rho^{\mathrm{bulk}}_{\mathrm{PDMS}}$is the bulk density of PDMS on PDMS rich-PIB poor side. The shape of density profile for the other two systems PnBMA/PDMS/CO_2 and PnBMA/PDMS/C_2H_6 are similar to the density profile of PIB/PDMS/CO_2. The interfacial thickness is defined similarly.

Figures 4.1-4.6 illustrate that the interfacial tension and interfacial thickness vary with pressure for system PDMS[19]/PIB[20]/CO_2, PDMS[21] /PnBMA[22]/C_2H_6 and PDMS/PnBMA/CO_2. In each case, the interfacial thicknesses increase monotonically with pressure and double at high pressure ($\sim$16 MPa) relative to those without solvent. The interfacial tension decreases monotonically with pressure for system PDMS/PIB/CO_2, PDMS/PnBMA/C_2H_6, but there is a shallow minimum in the interfacial tension for PDMS/PnBMA/CO_2 in the neighborhood of the theoretical critical pressure ($\sim$ 8 MPa).

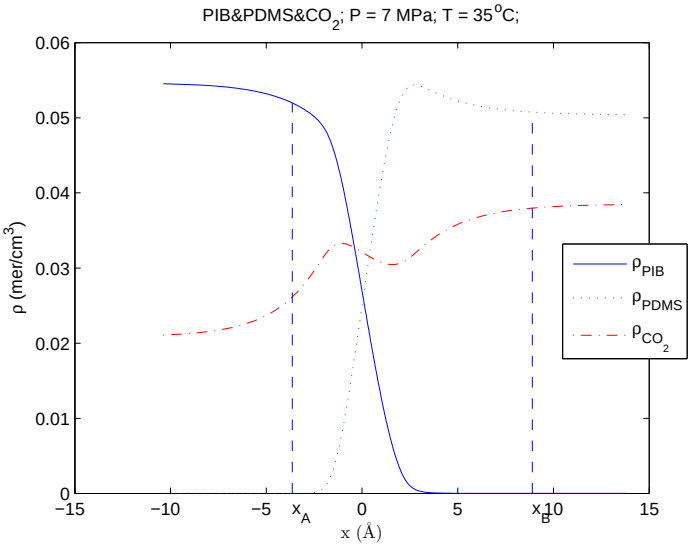

Figure 4.1: Interfacial density profile for system PIB/PDMS/CO_2

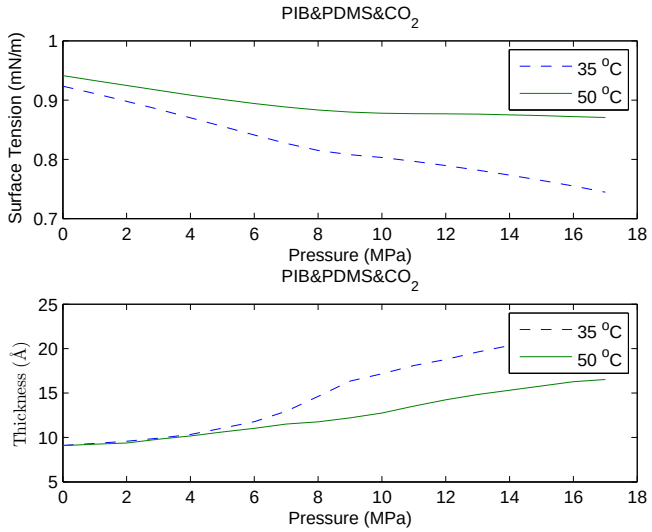

Figure 4.2: Interfacial properties for PIB/PDMS/CO_2 *vs.* pressure

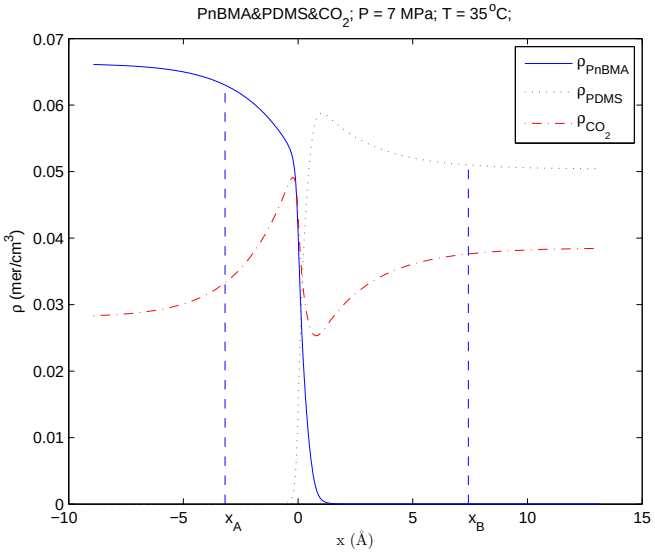

Figure 4.3: Interfacial density profile for system PnBMA/PDMS/CO_2

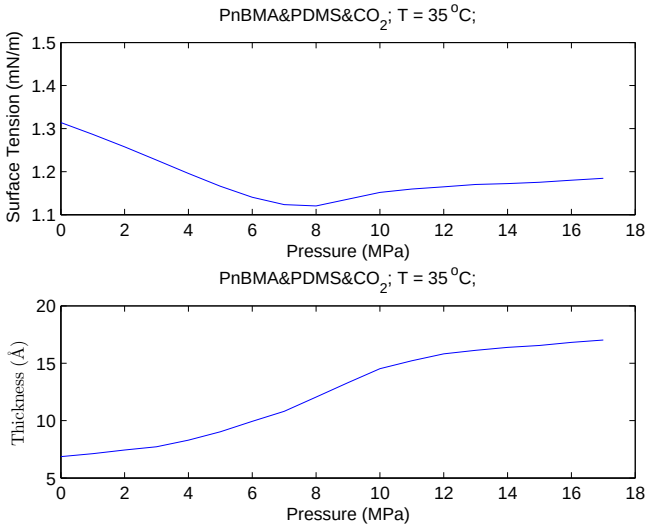

Figure 4.4: Interfacial properties for PnBMA/PDMS/CO_2 *vs.* pressure

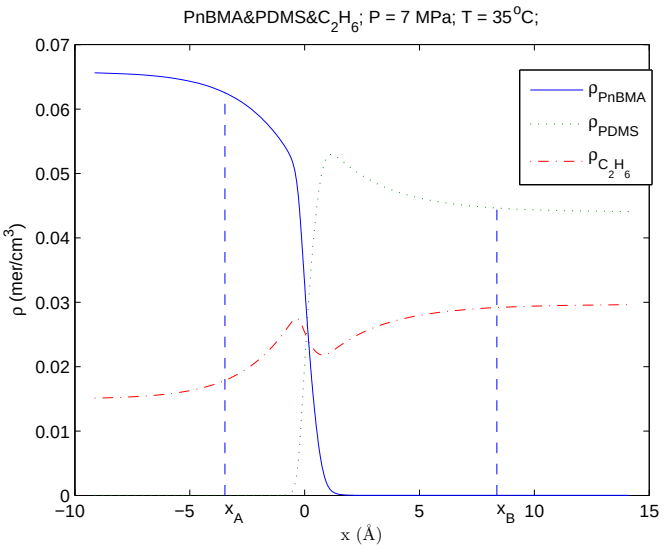

Figure 4.5: Interfacial density profile for system PnBMA/PDMS/C_2H_6

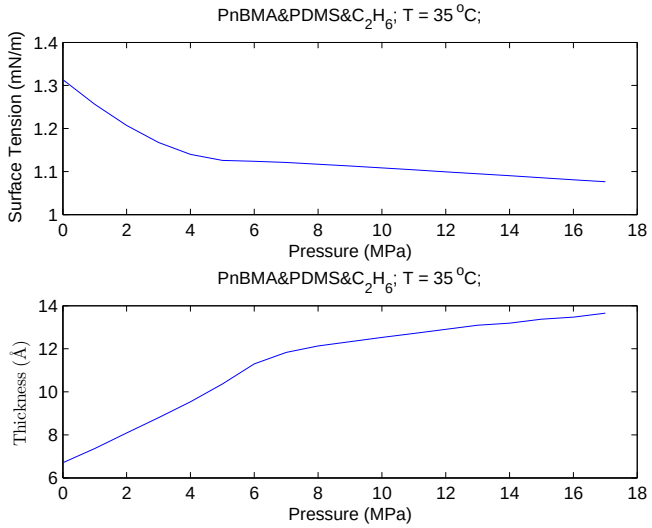

Figure 4.6: Interfacial properties for PnBMA/PDMS/C_2H_6 *vs.* pressure

Table 4.1: Binary interaction parameter

		ζ	δ	T (°C)	Ref.
PDMS	CO_2	0.9512	0.0154	35	[19]
PIB	CO_2	0.8996	0.0266	35	[20]
PnBMA	CO_2	0.9246	-0.012	35	[22]
PnBMA	C_2H_6	0.9792	-0.0125	35	[22]
PDMS	C_2H_6	0.9832	-0.0198	35	[21]

The pressure range (0-17 MPa) covers the sub-critical and supercritical region of CO_2 and C_2H_6. The interfacial properties, including interfacial tension and interfacial thickness, do not show any significant change near the respective critical pressures. As can be seen in Figure 4.2, the compatibilization effect of the supercritical fluid decreases with increasing temperature, i.e., the reduction in interfacial tension is not as effective at higher temperatures. This is consistent with the general solubility behavior of gases in polymers: gas solubility decreases with increasing temperature.

We also see preferential interfacial adsorption of PDMS in all cases. The surface tension of PDMS is lower than those of PIB and PnBMA. As a general rule of thumb, the lowest surface tension component is always preferentially adsorbed to the interface. The theoretical surface tension calculated in this work at 35 °C is: PDMS 14.7 mN/m, PIB 24.3 mN/m, PnBMA 26.6 mN/m.

4.4 Conclusion

In this paper, a combination of the gradient theory of inhomogeneous systems and the Sanchez-Lacombe equation of state was used to investigate the effect of a supercritical fluid on the interface of polymer blends, especially the effect of high compressibility of supercritical fluid to the compatibilization of two incompatible polymers. We calculate the interfacial density profile, interfacial thickness and interfacial tension between the two polymers with and without supercritical fluid. The interfacial tension decreases and the interfacial thickness increases with high pressure supercritical fluid for the blend systems we have investigated. These results suggest the idea that the mechanical properties of an immiscible polymer blends can be improved by exposure to a supercritical fluid. No enhancements or deleterious effects on compatibilization were observed in the neighborhood of the critical pressure.

4.5 Bibliography

[1] Buxton, G. A.; Balazs, A. C. *Interface Science* **2003**, *11*(2), 175–186.

[2] Benkoski, J. J.; Fredrickson, G. H.; Kramer, E. J. *Journal of Polymer Science Part B-Polymer Physics* **2002**, *40*(20), 2377–2386.

[3] Schnell, R.; Stamm, M.; Creton, C. *Macromolecules* **1998**, *31*(7), 2284–2292.

[4] McHugh, M. A.; Krukonis, V.; 2nd ed., 1994.

[5] Elkovitch, M. D.; Tomasko, D. L.; Lee, L. J. *Polymer Engineering and Science* **1999**, *39*(10), 2075–2084.

[6] Eugene, H.; Yukiko, T. *The Journal of Chemical Physics* **1972**, *56*(7), 3592–3601.

[7] Helfand, E.; Sapse, A. M. *Journal of Chemical Physics* **1975**, *62*(4), 1327–1331.

[8] Helfand, E.; Tagami, Y. *Journal of Polymer Science Part B-Polymer Physics* **1996**, *34*(12), 1947–1952.

[9] Hong, K. M.; Noolandi, J. *Macromolecules* **1981**, *14*(3), 736–742.

[10] Hong, K. M.; Noolandi, J. *Macromolecules* **1981**, *14*(3), 727–736.

[11] Rowlinson, J. S. *Journal of Statistical Physics* **1979**, *20*(2), 197–244.

[12] Bongiorno, V.; Davis, H. T. *Physical Review A* **1975**, *12*(5), 2213–2224.

[13] Cahn, J. W.; Hilliard, J. E. *Journal of Chemical Physics* **1958**, *28*, 258–67.

[14] Poser, C. I.; Sanchez, I. C. *Macromolecules* **1981**, *14*(2), 361–70.

[15] Sanchez, I. C.; Lacombe, R. H. *Journal of Physical Chemistry* **1976**, *80*(21), 2352–2362.

[16] Wang, X.; Sanchez, I. C. *Langmuir* **2006**, *22*(22), 9251–9253.

[17] Walker, T. A.; Colina, C. M.; Gubbins, K. E.; Spontak, R. J. *Macromolecules* **2004**, *37*(7), 2588–2595.

[18] Poser, C. I.; Sanchez, I. C. *Journal of Colloid and Interface Science* **1979**, *69*(3), 539–548.

[19] Pope, D. S.; Sanchez, I. C.; Koros, W. J.; Fleming, G. K. *Macromolecules* **1991**, *24*(8), 1779–1783.

[20] Chang, S. H.; Park, S. C.; Shim, J. J. *Journal of Supercritical Fluids* **1998**, *13*(1-3), 113–119.

[21] Merkel, T. C.; Bondar, V. I.; Nagai, K.; Freeman, B. D.; Pinnau, I. *Journal of Polymer Science Part B-Polymer Physics* **2000**, *38*(3), 415–434.

[22] Nadakatti, S. M.; Kim, J. H.; Stern, S. A. *Journal of Membrane Science* **1995**, *108*(3), 279–291.

Chapter 5

Ordering in Asymmetric Block Copolymer Films by a Compressible Fluid

We examine the morphological structures of asymmetric poly(ethylene oxide)-b-poly(1,1'-dihydroperflurooctyl methacrylate) (PEO-b-PFOMA) thin films upon annealing in a compressible fluid, supercritical CO_2. The strong affinity between PFOMA and CO_2 is found to induce phase segregation when annealing PEO-b-PFOMA films at the same temperature as compared with vacuum. In vacuum, PEO-b-PFOMA films remain disordered from 80-180 °C, whereas in supercritical CO_2 at 13.9 MPa, an upper order-disorder transition (UODT) between 116 and 145 °C is found. In supercritical CO_2, the observed ordered structure is layers of PEO spheres embedded in the matrix of PFOMA, followed by a brush layer, in which PEO wets the substrate. The swelling isotherms of PFOMA and PEO in CO_2 are correlated with the Sanchez-Lacombe equation of state (S-L EOS) to estimate the interaction parameters, $\chi_{\mathrm{PFOMA-CO_2}}$ and $\chi_{\mathrm{PEO-CO_2}}$. The phase segregation (order) induced by CO_2 relative to vacuum at a given temperature is explained in terms of two

[1]Yuan Li did the experimental part of this work

[2]Reprinted with permission from Yuan Li; Xiaochu Wang; Isaac C. Sanchez; Keith P. Johnston and Peter F. Green *J. Phys. Chem. B* **2006**, 110(51). Copyright ©2006 American Chemical Society

factors: (1) copolymer volume fraction upon dilution with CO_2, ϕ, and (2) the relative interaction parameter, $\Delta\chi = |\chi_{\mathrm{PFOMA-CO_2}} - \chi_{\mathrm{PEO-CO_2}}|$. The latter factor favors order and is dominant at low temperatures over the ϕ factor, which always favors disorder. At high temperatures (above the T_{ODT}), the preferential swelling of PFOMA by CO_2 is less pronounced ($\Delta\chi$ decreases), and the copolymer is disordered.

5.1 Introduction

In recent years, rapid progress has been reported toward exploiting microphase segregation in block copolymer (BCP) thin films to create periodically ordered nanopatterned substrates for potential applications such as nanolithography and "bottom" up microelectronic device fabrication [1, 2]. Efforts have been largely devoted to the control of the orientation and lateral ordering of microphase segregated domains using external and internal forces [1–7]. Compressible fluids, such as supercritical CO_2, have been widely used in many polymer related processes and provide certain advantages [8]. Unlike conventional liquid solvents, the density, and hence the "solvent strength" of supercritical CO_2, can be tuned by small variations in pressure, temperature, or both. This tunability, along with the low interfacial tension and high diffusion coefficient, makes supercritical CO_2 a strategic solvent to pattern BCP templates at relatively low temperatures. For example, Pai et al. used supercritical CO_2 as a processing medium for the infusion and condensation of silicon alkoxides in mesophase-separated BCP templates [9]. Li et al. demonstrated

that the core-shell structure of BCP micelles in thin films can be inverted by supercritical CO_2 and that the size of micellar cores can be finely tuned by modifying CO_2 activities. This inversion was utilized to guide the segregation of presynthesized Au nanopaticles in one of the domains, and thus, inorganic nanocrystals were sequestered into multilayered BCP templates.

The effects of supercritical CO_2 on the compatibility of bulk BCPs and polymer blends have been investigated [10–12]. Both enthalpic driven upper order-disorder transition (UODT) and entropic driven lower disorder-order transition (LDOT) temperatures were found to decrease in supercritical CO_2 [10–12]. The presence of supercritical CO_2 on the free surface of thin BCP films can strongly influence the interfacial interactions, effectively modify the kinetics of phase segregation, and substantially affect the wetting behavior. RamachandraRao et al. showed that sorption of supercritical CO_2 highly enhanced the ordering kinetics of high molecular weight, symmetric, polystyrene-b-polymethylmethacrylte (PS-b-PMMA) films (~ 0.3 μm) and that the wetting symmetry was reversed in supercritical CO_2 compared with vacuum [13]. Arceo et al. examined much thinner, symmetric, PS-b-PMMA films (~ 30 nm) and showed that supercritical CO_2 decreased the order-disorder transition temperature, T_{ODT}, and favored microphase segregation [14]. Specifically, the ordering transition shifts from $(\chi N)_{\mathrm{ODT}}$>10.5 in the bulk, where N is the degree of polymerization and χ is the Flory-Huggins interaction parameter, to $(\chi N)_{\mathrm{ODT}}$=7.94 for films thinner than 30 nm on silicon oxide. Theoretical work by Shah et al. indicates that the solvent compressibility and selectivity

toward one block can significantly affect the ordering of copolymer thin films [15].

In this study, we examine the influence of supercritical CO_2 on the ordering of highly asymmetric bulk and thin film PEO-b-PFOMA copolymers. We show that, in vacuum, PEO-b-PFOMA films are disordered in the temperature range of 80-180 °C and that in supercritical CO_2, at a pressure of 13.9 MPa, PEO-b-PFOMA films undergo an ODT between 116 and 145 °C. The ordered structure is composed of layers of PEO spheres embedded in the matrix of PFOMA. This structure resides on a brush layer of PEO chains in contact with the substrate. The phase segregation (order) induced by CO_2 is explained in terms of two factors: (1) copolymer volume fraction upon dilution with CO_2, ϕ, and (2) the relative interaction parameter, $\Delta\chi = |\chi_{\mathrm{PFOMA-CO_2}} - \chi_{\mathrm{PEO-CO_2}}|$. The Sanchez-Lacombe equation of state (S-L EOS) is used to fit the swelling isotherms of PFOMA and PEO in CO_2 and to estimate quantitatively the two interaction parameters, $\chi_{\mathrm{PFOMA-CO_2}}$ and $\chi_{\mathrm{PEO-CO_2}}$.

5.2 Experimental Section

5.2.1 Materials and Thin Film Preparation

The molar weight of the PEO block is 5 kg/mol, and that of the PFOMA block is 52 kg/mol as determined by ^{1}H NMR. Other properties of this copolymer are summarized in Table 5.1 [16, 17]. Since the volume fraction of the PEO block is 0.12, the equilibrium microphase segregated structure is

Table 5.1: Characteristics of PEO and PFOMA in the Diblock

parameters	PEO	PFOMA
M_n (kg/mol)	5	52
T_g (°C)	$< RT$	50
T_m (°C)	63	NA
M_o (g/mol)	44	468
N	114	111
γ (dyn/cm)	43	<11
f (volume fraction)	0.12	0.88

expected to be spheres of PEO embedded in a continuous matrix of PFOMA [18, 19].

Small-angle X-ray scattering (SAXS) measurement was performed on bulk PEO-b-PFOMA, and the experimental procedure is described as the following. Sufficient material to fill a 3 mm × 10 × mm × 1 mm deep cavity was sealed in a stainless steel sample holder using a pair of 0.001 in. thick Kapton windows. Kapton windows do not contribute significantly to the scattering in the region of interest. The prepared sample was then loaded into a temperature controlled heating block and placed under the X-ray beam (Cu Kα) of a Molecular Metrology SAXS instrument. The geometry of the experimentally afforded sampling d-spacing is from about 3.5 to 70 nm.

To prepare thin film samples, the diblock was first dissolved using a cosolvent mixture of 1,1,2-trichlorotrifluroethane (Freon- 113) and chloroform. The resulting transparent solutions had a concentration of 0.5-1 wt % polymer and 15-25 wt % chloroform. Thin films were prepared by spin casting the so-

lutions onto silicon wafers (Wafer World Inc.) with a thin native oxide layer. The thicknesses of the films were measured by spectroscopic ellipsometry (J. A. Woollam Co., Inc.). Different thicknesses (30-80 nm) were obtained by controlling the spin rate and modifying the solution concentrations. The samples were then annealed in either vacuum ovens or supercritical CO_2 environments. Topography analyses of the resulting films were performed in contact mode using Autoprobe CP scanning force microscopy (SFM) equipment from Park Instruments. For some samples, SFM height and phase images were obtained simultaneously in tapping mode using a Nanoscope IV/Dimension 3100 (Digital Instruments).

5.2.2 Supercritical CO_2 Annealing

The samples were loaded into a fixed volume cell, which was subsequently sealed and pressurized with carbon dioxide (Air Products, >99.999) using a manual pressure generator (High-Pressure Equipment Co.). The pressure was controlled with a strain gauge pressure transducer (Sensotec) calibrated to within $\pm 7 \times 10^{-3}$ MPa. Typically, the temperature was controlled to ± 0.1 °C by immersing the pressure cell into a water bath equipped with a temperature controller (Julabo, Inc.). For high temperature (above 100 °C) experiments, the pressure cell was wrapped with a heating tape connected to a temperature controller (Omega Engineering, Inc). The glass transition temperature (T_g) of PFOMA is 50 °C, and the melting temperature (T_m) of PEO is about 63 °C (T_g for PEO is below room temperature) in vacuum. Since all

transition temperatures should be even more depressed in CO_2, the diblock was in a rubbery state under all conditions studied (60-145 °C and at the supercritical CO_2 pressure of 13.9 MPa). After an annealing period (varying from 10 h to 10 d), the cell was cooled to approximately 25 °C and depressurized by venting supercritical CO_2 as a vapor from the top. In the process of depressurization and cooling, the films return to the glassy state and the morphology was frozen.

5.2.3 In-situ Swelling Experiments

Spectroscopic ellipsometry (J. A. Woollam Co., Inc.) was used to measure the in-situ swelling of PFOMA (M_n=100 kg/mol) homopolymer films (thicknesses between 100 and 120 nm) in supercritical CO_2. The detailed experimental apparatus and procedures are described elsewhere [20]. The swelling percentage was determined by assuming uniaxial swelling

$$\mathrm{Sw\%} = \frac{\mathrm{h} - \mathrm{h_0}}{\mathrm{h_0}} \times 100\% \tag{5.1}$$

Here, h is the thickness of the swollen film, and h_0 is the initial thickness of the polymer film determined by spectroscopic ellipsometry at 0 psig.

5.3 Results

5.3.1 Absence of Order in Vacuum *vs.* an Order-Disorder Transition in supercritical CO_2 in the Same Temperature Range

In BCP thin films, phase segregated domains typically align parallel to the surfaces due to the preferential interactions between one block and the

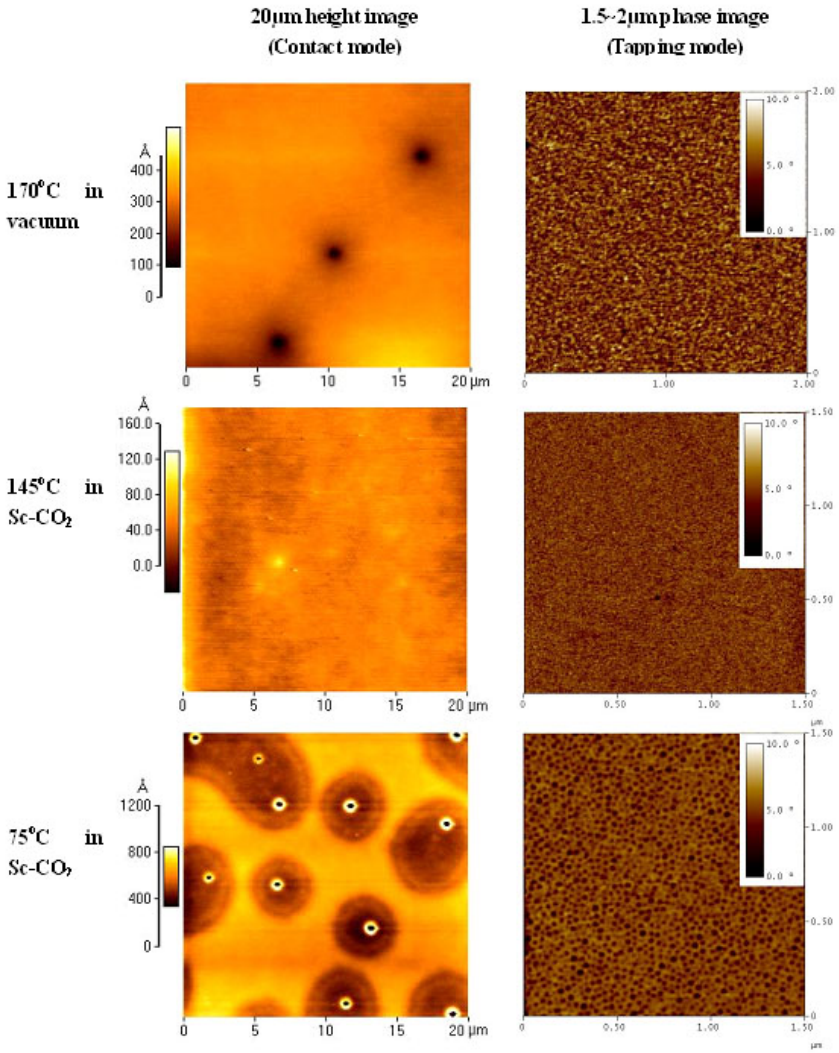

Figure 5.1: SFM images for PEO-b-PFOMA films after annealing under various conditions. The images on the left column are 20 μm height images from contact mode SFM, whereas the images on the right column are 1.5 $\sim$ 2μm phase images from tapping mode SFM. Detailed information for each image is: (a, b) h=67nm after annealing in vacuum ovens at 170 °C for 240 hours; (c, d) h=57 nm after annealing at CO_2, 145 °C, 13.8 MPa for 48 hours; (e, f) h=55 nm after annealing at CO_2, 75 °C, 13.8 MPa for 76 hours.

interfaces (both free surface and the substrate) [21–25]. For symmetric BCP films, if L is the size of the periodic spacing, then the thickness of the brush layer, L_0, in contact with the substrate, is normally L or $L/2$ for symmetric and asymmetric wetting cases, respectively [21]. If the initial film thickness deviates from the $nL + L_0$ criterion [21], then the excess material will form a discontinuous layer with either holes or islands of height L. This so-called terrace structure has been widely used to identify the ordering of both symmetric and asymmetric BCP films [21–23].

The eventual structure of the film is allowed to develop after spin-casting from solution onto the substrate and subsequently annealing under either vacuum or supercritical CO_2 conditions. Figure 5.1 compares the topography of PEO-b-PFOMA films under different annealing conditions. In the first set of experiments, the films (30-80 nm) were annealed in vacuum ovens at various temperatures (in the range of 80-180 °C) and representative images are shown in Figure 5.1a and b. The absence of any terrace structure in the height image (a) indicates that the diblock is in a disordered state. The phase image (b) does not show any particular nanoscopic structure, further supporting the observation of the height image that the PEO-b-PFOMA films are phase miscible under the experimental vacuum conditions. It is noteworthy that no dewetting droplets associated structural instability was observed for PEO-b-PFOMA films after an extensive annealing period in the vacuum ovens. This stability is not surprising since both PEO and the carbonyl group in PFOMA are known to have strong interactions with the polar Si/SiOx

substrate [24, 26].

In the second set of experiments, the PEO-b-PFOMA films were annealed under supercritical CO_2 conditions at 13.9 MPa, over a temperature range of 60-145 °C. This temperature range was chosen so that supercritical CO_2 annealing temperatures were kept above the melting temperature of the PEO block [17], given complications that may arise from crystallization. The film shown in Figure 5.1c and d was annealed at 145 °C for 48 hours. The absence of either a mesoscopic terrace-like or nanoscopic spherical structures indicates that PEO-b-PFOMA films are also disordered under this condition. However, as the supercritical CO_2 annealing temperature decreases, the films start to become ordered. Figure 5.1e and f are the topography of a PEO-b-PFOMA film after annealing at 75 °C and 13.9 MPa for 76 hours. Evidently, Figure 5.1e shows a discontinuous layer with holes, suggesting that the diblock is in an ordered state. In addition, random arrays of PEO spheres embedded in the matrix of PFOMA were observed in Figure 5.1f. Consistent with previous studies [27, 28], the PEO block appears in a darker color in the phase contrast SFM images, owing to its much lower glass transition temperature compared with PFOMA. Finally, it is noteworthy that similar images as Figure 5.1e and f were obtained for samples annealed in supercritical CO_2 in the temperature range of 60-116 °C at 13.9 MPa.

To further prove the absence of order after vacuum annealing, SAXS measurements were performed on bulk PEO-b-PFOMA samples to explore any potential ODT over a broader temperature range (100-280 °C in 30-40 °C

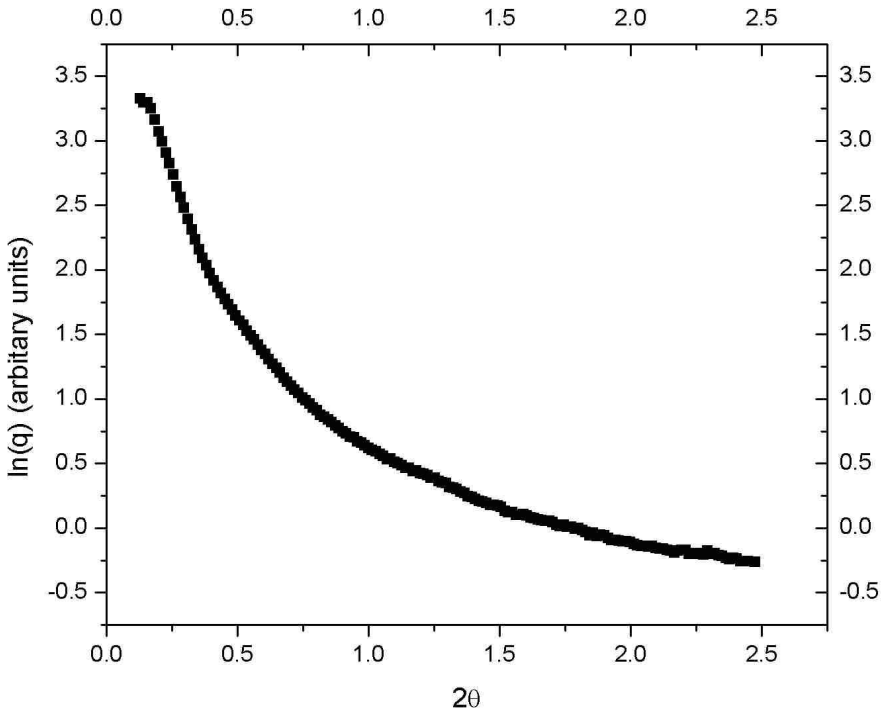

Figure 5.2: A representative small angle X-ray scattering (SAXS) spectrum of bulk PEO-b-PFOMA at 135 °C

increments). However, as shown by a representative spectrum (Figure 5.2), no scattering peak can be found from the intensity *vs.* scattering angle profile. The scattering intensity contrast between PEO and PFOMA blocks is expected to be strong due to the large difference in the X-ray atomic scattering factors for H and F atoms. Therefore, this absence of scattering peak suggests that no ordering could be identified over the experimental temperature range.

In summary, in vacuum, SAXS shows that bulk PEO-b-PFOMA diblock remains disordered at 100-280 °C and, consistently, SFM shows that PEO-b-PFOMA thin films are disordered at 80-180 °C. On the other hand, upon annealing in supercritical CO_2 at 13.9 MPa, an ODT was found between 116 and 145 °C.

Before ending this section, it is noteworthy that in Figure 5.1f, the PEO spheres appear to only have a short-range liquidlike order. The absence of any long-range order is an intrinsic property associated with asymmetric BCP systems. Unlike symmetric BCPs, which go directly from a disordered state to an ordered lamellar state, asymmetric BCPs were found to follow the path from a disordered state, to a liquidlike array of spheres, and to a perfectly aligned crystal structure of spheres [25, 29]. Therefore, two first-order phase transitions are believed to exist in asymmetric BCPs, one being the conventional ODT and the other being the "spatial disordering" [29] or lattice disorder-order transition [25]. Given the lack of perfectly aligned spheres, the experimental temperature range of 60-116 °C in supercritical CO_2 at 13.9 MPa is below the T_{ODT} while it is above the corresponding spatial disorder

Table 5.2: Measured layer height for PEO-b-PFOMA Films after Supercritical CO_2 Annealing

Condition	L_0 (nm)	L_1 (nm)	L_2 (nm)
60 °C, 13.8 MPa	10.3±1.1	24.2±1.8	23.0±2.0
75 °C, 13.8 MPa	11.7±1.2	23.8±2.1	22.7±3.7
116 °C, 13.8 MPa	11.3±2.2	22.6±3.1	19.1±3.3

transition temperature.

5.3.2 Periodic Spacing of Ordered PEO-b-PFOMA Films in Supercritical CO_2

To obtain a height profile of the PEO-b-PFOMA films in the z direction, films were scratched prior to annealing to expose the underlying substrate, and numerous line scans were taken near the scratch. However, as has been observed by Reiter et al. [26, 30], the PEO chains have a strong affinity with the polar Si/SiOx substrate. As a consequence, the scratch made prior to annealing will be covered by a thin brush layer once the polymer chains are given mobility to move under annealing conditions.

Figure 5.3a-c shows the representative SFM images and the corresponding line-scans on the edge of the scratches on PEO-b-PFOMA samples after annealing at different supercritical CO_2 temperatures at 13.9 MPa. Figure 5.3a shows a film after annealing at 145 °C for 48 hours, where no steps are observed near the scratch, further proving that the film is disordered. In Figure 5.3b and c, two steps can be clearly identified on the edge and the heights of each layer, L_1 and L_2, are measured based on the average of numerous line-

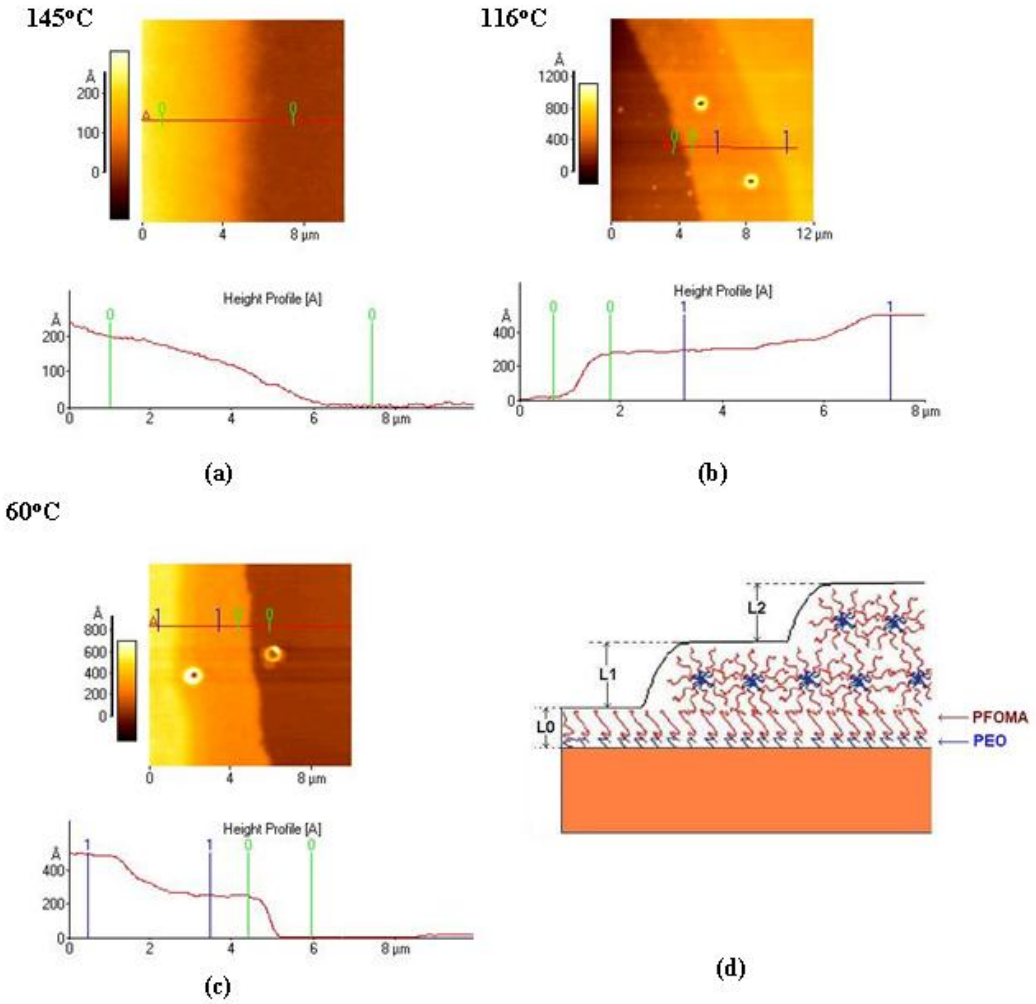

Figure 5.3: SFM images and the corresponding line scans for PEO-b-PFOMA films annealed in supercritical CO_2: (a) an h=46 nm film after annealing at CO_2, 145 °C, 13.8 MPa for 48 hours; (b) an h=57 nm film after annealing at CO_2, 116 °C, 13.8 MPa for 48 hours; (c) an h=47nm film after annealing at CO_2, 60 °C, 13.8 MPa for 30 hours. Notice that except (a), both (b) and (c) show formation of terrace near the scratch. (d) Schematic drawing of the layered structure in phase segregated PEO-b-PFOMA films.

scans as listed in Table 5.2. Moreover, several white spots, which are actually small holes with rims, are observed throughout Figure 5.3b and c as well as in Figure 5.1e. These white spots (0.5-1 μm in diameter) are the result of fast CO_2 diffusion from the interface between the films and substrate when the samples were abruptly depressurized to ambient conditions. Decreasing the depressurization rate reduces the number of depressions, or holes. Since CO_2 is expected to partially absorb on the substrate, the bottom of each depression is found to expose the underlying substrate. Therefore, the height difference between the brush layer covering the scratch and the bottom of these holes is used to determine the height of the brush layer, L_0.

Figure 5.3d shows a schematic drawing of the layered structure in phase segregated PEO-b-PFOMA films, where spheres of PEO are embedded in the matrix of PFOMA, consistent with Figure 5.1f. The PFOMA block, owing to its substantially lower surface tension, resides on the free surface. To determine which block remains in contact with the substrate, it is instructive to compare the size of L_0 with L_1 and L_2. If PFOMA, the majority block, wets the substrate, then the spherical phase structure can remain intact. Consequently, L_0 should be equivalent to L_1 and L_2 [22]. On the other hand, if PEO, the minority block, wets the substrate, then the diblock has to form a half-lamellar layer on the substrate; hence, the value of L_0 is approximately half of L_1 and L_2 [22]. On the basis of the above discussion and Table 5.2, it is evident that PEO resides on the substrate.

To prove the validity of our height measurement for each layer, the

$nL + L_0$ criteria is used to justify the formation of islands or holes in films that were annealed at 75 °C and 13.9 MPa for 76 hours (Figure 5.4). As shown in Table 5.2, at 75 °C, the corresponding values for measured L_0, L_1, and L_2 are 12, 24, and 23 nm, respectively. Accordingly, a stable layer would have a thickness of 12 + 24 + 23 = 59 nm. Thus, an $h = 63$ nm film (Figure 5.4a) can minimize its free energy by forming a 59 nm layer and then another discontinuous layer of islands on top. In the same fashion, for an $h = 55$ nm film (Figure 5.4b), the free energy of the system is minimized by forming a discontinuous layer, which is 59 nm in height and contains holes. Therefore, good agreement is found between the measured layer heights and the $nL + L_0$ criterion.

It is noteworthy that the "flowerlike" patterns observed in Figure 5.4 (indicated by the circles) are due to partial crystallization of the PEO block when quenching to room temperature. PEO is a semicrystalline polymer, and the crystallization of PEO films as well as PEO containing copolymer films has been examined [26, 28, 30]. The melting temperature depression for bulk PEO in supercritical CO_2 has also been explored [17]. In our study, to avoid the complication between crystallization and phase separation, the experimental CO_2 annealing temperatures are always kept above the melting temperature of PEO. However, after CO_2 annealing, the PEO-b-PFOMA films are subsequently quenched to room temperature for SFM imaging. During this abrupt quenching, PEO-b-PFOMA films can partially crystallize, forming the observed flowerlike patterns.

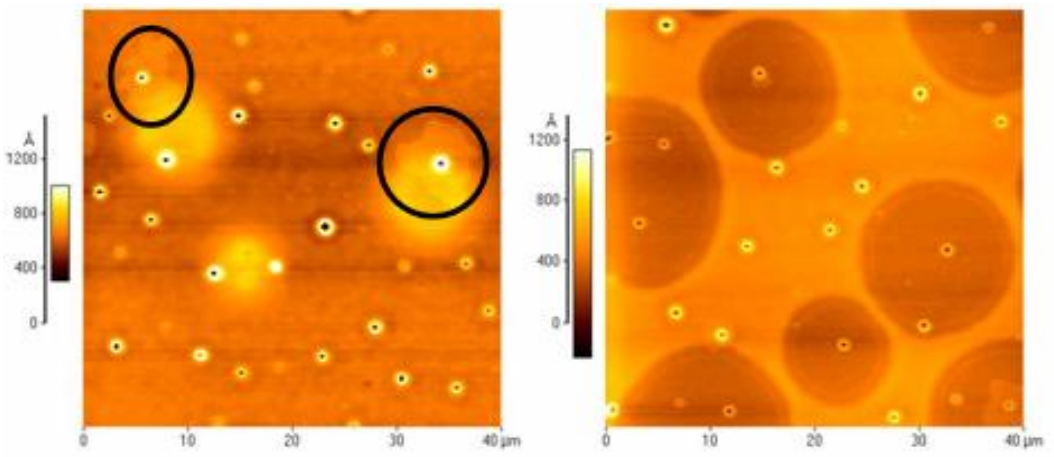

Figure 5.4: SFM topography of PEO-b-PFOMA films with thicknesses (a) h=63 nm and (b) h=55 nm after annealing at CO_2, 75 °C, 13.8 MPa for 76 hours. Notice that in Figure (a), the flower like pattern on the edge of the two big islands (marked by the circles) are the results of PEO chains crystallization after supercritical CO_2 annealing and subsequently quenching to ambient condition

5.3.3 Fitting of Swelling Isotherms for PFOMA and PEO in CO_2

In-situ sorption measurements were performed using spectroscopic ellipsometry for PFOMA films as shown in Figure 5.5a, where swelling isotherms of PFOMA are plotted against supercritical CO_2 activity to combine the effects of temperature and pressure. As has been discussed in our previous work [31], swelling of a rubbery polymer in supercritical CO_2 only depends on CO_2 activities. Because the T_g of PFOMA is only 50 °C under ambient conditions and is depressed under supercritical CO_2, the difference between the two PFOMA isotherms is within experimental error range. This superposed swelling *vs.* CO_2 activity also suggests that one can estimate the corresponding percent swelling at higher temperatures, given the corresponding CO_2 activities (shown in Figure 5.5b).

To estimate the change of $\Delta\chi = |\chi_{\mathrm{PFOMA-CO_2}} - \chi_{\mathrm{PEO-CO_2}}|$ with temperature, the Sanchez-Lacombe equation of state (S-L EOS) [32, 33] is used to fit the swelling isotherms using the nonlinear least-square method. Following the mixing rule proposed by Sanchez et al. and commonly used by many S-L EOS modeling papers [10, 34–36], we employ the following equations for the mixture of CO_2 (phase 1) and polymer (phase 2). Sanchez and Lacombe [33] derived a concentration dependent interaction parameter χ, which can be expressed as

$$\chi = \chi_1 + \chi_2\phi_2 + \chi_3\phi_2^2 + \cdots \tag{5.2}$$

Table 5.3 shows characteristic S-L EOS parameters used in our fitting

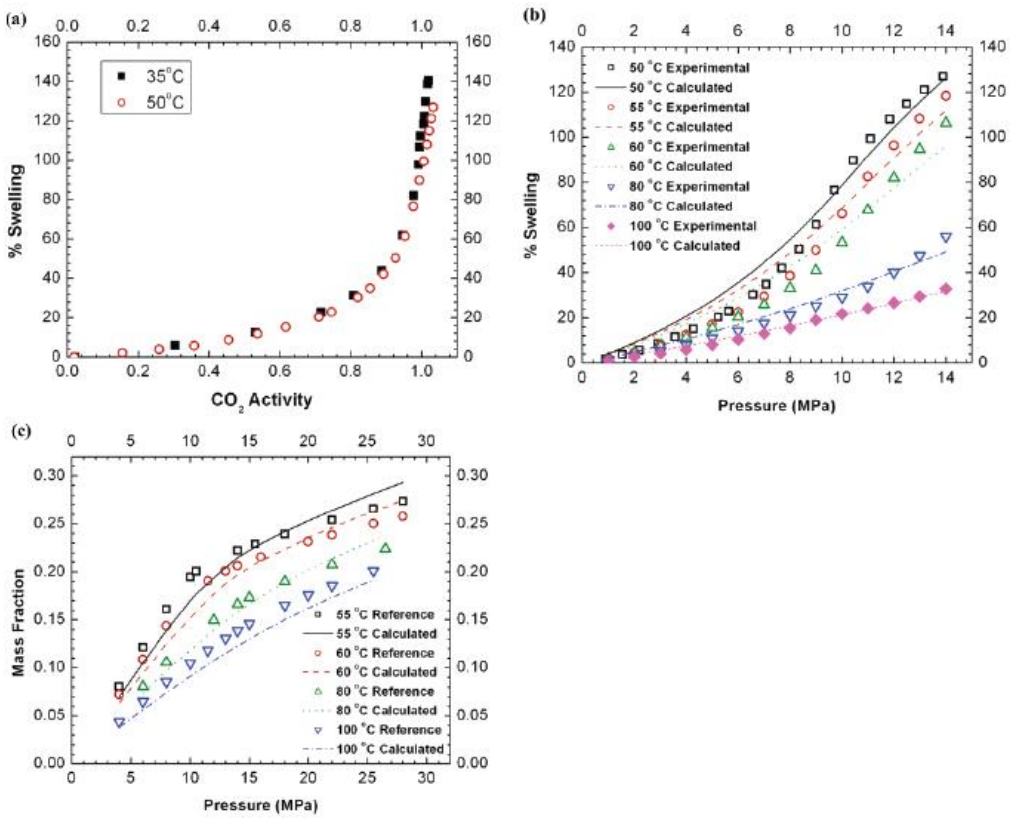

Figure 5.5: (a) Experimentally measured percent swelling as a function of CO_2 activity for PFOMA films ($h_0 \sim 110$ nm). (b) S-L EOS fitting of the experimental and extrapolated swelling isotherms for PFOMA films in supercritical CO_2. (c) S-L EOS fitting of the mass fraction of CO_2 in PEO based on the work by Weidner et al.

Table 5.3: Sanchez-Lacombe Pure Component Characteristic Parameters

component	T^* (K)	P^* (atm)	ρ^* (g/cm^3)	Reference
CO_2	283	6504	1.62	[37]
PFOMA	540.01	4399	1.677	[38]
PEO	658	4787	1.182	[39]

Table 5.4: Estimated Cohesive Energy Density from the Parameters in Table 5.3

	60 °C, 13.9 MPa		145 °C, 13.9 MPa	
component	$\tilde{\rho}$	CED (MPa)	$\tilde{\rho}$	CED (MPa)
CO_2	0.262	45.2	0.134	10.1
PFOMA	0.893	356	0.826	304
PEO	0.933	423	0.885	380

[37–39]. It is noteworthy that several sets of EOS parameters for CO_2 are available [40]. We choose the one that gives a critical CO_2 temperature (T_c) close to 31 °C. Additionally, P^* is known to be related to the cohesive energy density (CED) [41]. Both CO_2 and CO_2-philic polymers possess inherently low CEDs; however, Table 5.3 shows that P^* for CO_2 is fairly large and even exceeds that of PEO. This discrepancy can be explained by Table 5.4, which estimates the CED values based on the equation of state approach as derived by Panayiotou [42]

$$\text{CED} = \delta^2 = \tilde{\rho}^2 P^* \tag{5.3}$$

Here, δ is the solubility parameter. From Table 5.4, it is clear than even though CO_2 has a relatively large P^*, it also has a much lower reduced density ($\tilde{\rho}$) than those of the polymers. Thus, the estimated CED for CO_2 is small as expected.

Figures 5.5b shows that the S-L EOS fits the PFOMA swelling isotherms in CO_2 at temperatures from 50 to 100 °C with good accuracy. Phase equilibrium of the PEO-CO_2 system has been examined by many groups [35, 43–45]. Weidner et al. measured the mass fraction of CO_2 in PEO (4 kg/mol) at 55,

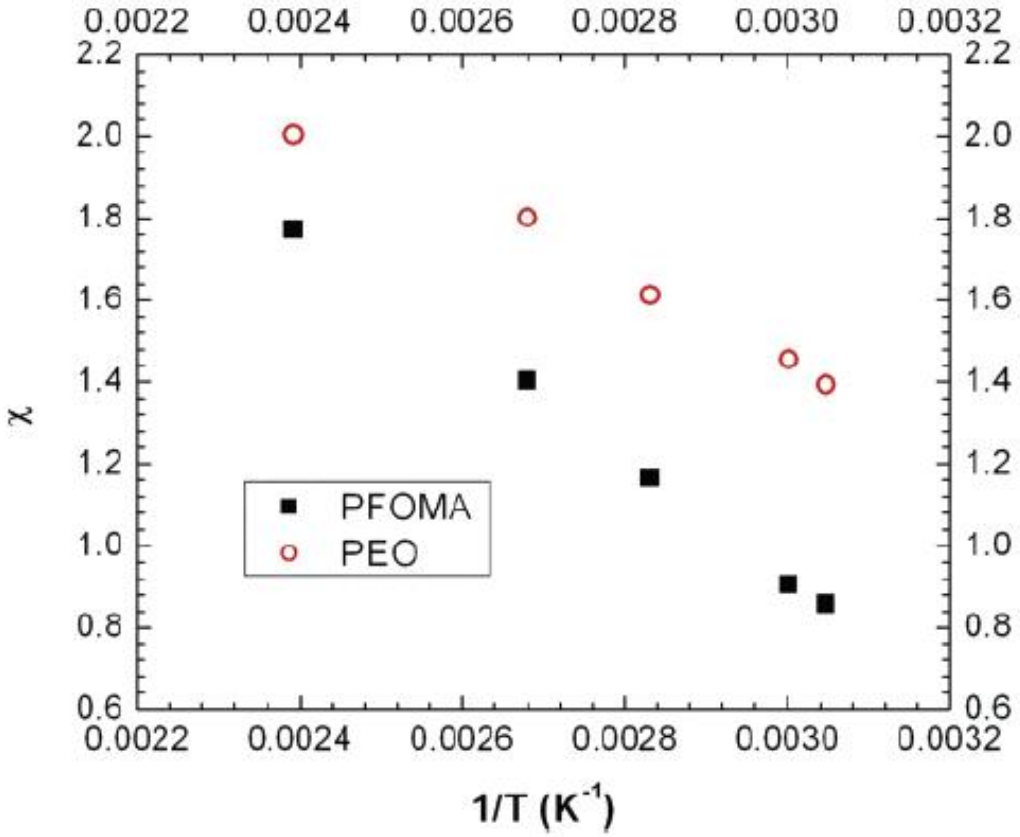

Figure 5.6: Calculated interaction parameters, PFOMA-CO_2 and PEO-CO_2, *vs.* temperature ($1/T$).

60, 80, and 100 °C and suggested that the solubility of CO_2 in PEO is almost independent of the PEO molar weight [43]. Similar results were obtained by Gourgouillon and co-workers [35]. We fit Weidner et al.'s data [43] for the four available temperatures, as shown in Figure 5.5c. It is noteworthy that Gourgouillon et al. [35] also modeled Weidner et al.'s data with the S-L EOS, but with a different set of CO_2 EOS parameters.

Table 5.5 summarizes the values of k_{12} fitted from the swelling isotherms and the corresponding χ values calculated at all temperatures. First, as expected, the S-L EOS calculated values for PFOMA-CO_2 are always lower than those for PEO-CO_2, suggesting that the interaction between PFOMA and CO_2 is more favorable. Second, the observed increase in χ with increasing temperature indicates that the interaction between polymers and CO_2 becomes less favorable, consistent with the decreasing CO_2 solubility in polymers with increasing temperature. This trend is opposite to the temperature dependence of classic χFH and is the reason why the simplified Flory-Huggins theory does not explain the commonly observed lower critical solution temperature (LCST) behavior in polymer-solvent systems. Third, as the CO_2 temperature increases, the value of $\Delta\chi = |\chi_{\mathrm{PFOMA-CO_2}} - \chi_{\mathrm{PEO-CO_2}}|$ decreases, suggesting that CO_2 becomes less of a selective solvent toward PFOMA. In Figure 5.6, the calculated χ values for both PFOMA-CO_2 and PEO-CO_2 are plotted versus $1/T$ and the trend of decreasing difference in χ as the temperature increases is clearly demonstrated.

5.4 Discussion

It is well-known that the phase diagram of a diblock copolymer (A-b-B) is typically determined by the interaction parameter, χ_{AB}, the total number of monomers that compose the chain, N, and the volume fraction of one block, f [46, 47]. At a given f, when $\chi_{\mathrm{AB}}N$ exceeds the corresponding critical value, the diblock can change from a disordered state to an ordered state. For example,

the critical $\chi_{\mathrm{AB}}N$ is 10.5 for f=0.5. Figure 5.7a illustrates schematically the effects of adding a neutral or selective solvent on the $\chi_{\mathrm{AB}}N$ versus f_{A} phase diagram of a diblock copolymer. Generally speaking, adding a neutral solvent is equivalent to a vertical trajectory, whereas adding a selective solvent is equivalent to a diagonal trajectory [48]. These effects will be examined in detail next.

When an A-b-B copolymer is dilated in a solvent, the effective interaction parameter will change to [48]

$$\chi_{eff} \sim \phi(\chi_{AB} + \Delta\chi) \sim \phi(\chi_{AB} + |\chi_{AS} - \chi_{BS}|) \tag{5.4}$$

Here, ϕ is the volume concentration of the copolymer in the solvent and $\Delta\chi$ is the difference between the A-solvent and B-solvent interaction parameters. For the case of a neutral solvent, $\Delta\chi \sim 0$ and, consequently,

$$\chi_{eff}N \sim \phi\chi_{AB}N \tag{5.5}$$

Thus, when adding a neutral solvent into a BCP system (ϕ <1), $\chi_{\mathrm{eff}}N$ decreases and the system may change from an ordered state to a disordered one. In other words, neutral solvent can effectively screen the unfavorable segmental contacts between the A and B blocks and can enhance phase compatibility. Because CO_2 can be considered as a neutral solvent for the two systems examined by Vogt and co-workers [10, 11], it is not surprising that CO_2 induces phase compatibility relative to vacuum. For example, for the diblock of poly(styrene-bisoprene) [10], Vogt et al. showed that the degrees of

swelling for polystyrene and polyisoprene at 35 °C are very similar, indicating that CO_2 interacts almost equally with both blocks.

However, the effects of a selective solvent on the compatibility of BCP systems can be complicated due to the interplay between ϕ and $\Delta\chi$. If we assume that the selective solvent preferentially swells the B block, then the volume fraction of the A block and the effective interaction parameter will change, accordingly [48]

$$f'_A \sim f_A\phi \tag{5.6}$$

$$\chi_{eff}N \sim \phi(\chi_{AB} + \Delta\chi)N \sim \phi(\chi_{AB} + |\chi_{AS} - \chi_{BS}|)N \tag{5.7}$$

In many cases, the presence of a large difference between the two polymer-solvent interaction parameters ($\Delta\chi$ is large and positive) raises $\chi_{\text{eff}}N$ from a disordered state into an ordered state. In other words, if the $\Delta\chi$ effect dominates the contribution resulting from a ϕ less than unity, then phase segregation can be induced by adding selective solvents. In addition, according to equation 5.6, adding a selective solvent for block B can lead to a significant decrease in the volume fraction of the A block, f_{A}. As a consequence, the decrease in f_{A} can cause a change in the equilibrium phase structure. For instance, Hanley et al. observed a sequence of phase changes from lamella (L) to perforated layer (PL) to gyroid (G) to cylinder (C) as the dilation of a slightly selective solvent to poly(styrene-bisoprene) [48].

Now, we can apply the above discussion to the PEO-b-PFOMA system annealed in supercritical CO_2 conditions. On the basis of equation 5.6, selective swelling of PFOMA by CO_2 decreases the effective volume fraction of the

Table 5.5: S-L EOS Fitting Results for PFOMA and PEO in supercritical CO_2

	PFOMA		PEO		
T (°C)	k_{12}	χ	k_{12}	χ	$\Delta\chi$
50	-0.0739	0.82			
55	-0.0765	0.86	-0.0247	1.39	0.53
60	-0.0758	0.90	-0.0237	1.46	0.56
80	-0.0580	1.17	-0.0300	1.61	0.44
100	-0.0461	1.40	-0.0386	1.80	0.40
145	-0.0331	1.77	-0.0498	2.00	0.23

PEO block (f'_{PEO} decreases). However, since f_{PEO} already lies in the spherical phase region in vacuum, further decreasing it will not change the equilibrium phase structure. In addition, according to equation 5.7, CO_2 annealing introduces two competing terms to $\chi_{\mathrm{eff}}N$: the overall copolymer volume fraction in the presence of CO_2, ϕ, which is less than 1 and a positive $\Delta\chi$, due to the preferential interaction between PFOMA and CO_2 [41]. The observed CO_2 induced phase segregation relative to vacuum annealing at the same temperature suggests that the $\Delta\chi$ effect is dominant; therefore, $(\chi_{\mathrm{eff}}N)_{\mathrm{CO_2}} > (\chi_{\mathrm{eff}}N)_{\mathrm{VAC}}$. This induced phase separation by the dominating $\Delta\chi$ effect has been observed in other systems, where a large disparity in the strength of polymer-solvent interactions exists [34, 49].

Next, we will discuss how changing the CO_2 temperature affects the phase diagram of PEO-b-PFOMA. Here, we will focus on the $\Delta\chi$ effect since that of ϕ is expected to be minor. Figure 5.7b illustrates schematically the effects of CO_2 as a selective solvent on the phase diagram of PEO-b-PFOMA. In vacuum, the diblock films are in disordered states at both temperatures

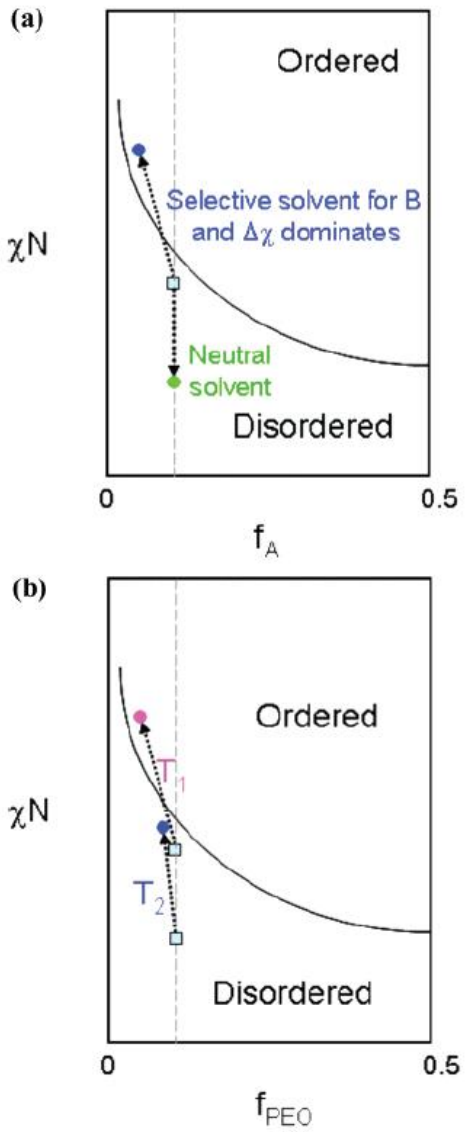

Figure 5.7: (a) Schematic phase diagrams for a typical diblock copolymer to show the effects of both neutral and selective solvents. (b) Schematic phase diagrams for PEO-b-PFOMA diblock copolymer ($T_1 < T_2$). Squares represent the case in vacuum, while dots represent the case in CO_2. At lower temperature T_1 (such as 116 °C), the diblock is disordered in vacuum and ordered in CO2 at 13.9 MPa, while, at higher temperature T_2 (such as 145 °C), the diblock is disordered in both vacuum and CO_2 at 13.9 MPa

($T_1 < T_2$); in supercritical CO_2 and at 13.9 MPa, the diblock is ordered at T_1 and disordered at T_2. As shown in Figure 5.7b, adding a selective solvent is equivalent to a diagonal trajectory [48] in the χN versus f phase diagram. At lower temperature T_1, the higher degree of CO_2 swelling reduces f_{PEO} more and thus the trajectory is steeper (the horizontal distance between the two ending points along the trajectory is larger). In addition, from Table 5.5, since $\Delta\chi$ decreases with increasing temperature, the increase in $\chi_{eff}N$ is more distinct at lower temperature T_1 (the vertical distance between the two ending points along the trajectory is larger). As a result, only at T_1, the change in $\chi_{eff}N$ is large enough to shift the diblock from a disordered state in vacuum to an ordered state in CO_2.

Finally, we would like to point out that in order to calculate the T_{ODT} of PEO-b-PFOMA in supercritical CO_2, one must consider the phase stability of a ternary system. In the case of a diblock copolymer in CO_2, the corresponding phase stability calculation of the ternary system is not available and thus will not be examined further. It is also evident that if χ_{eff} decreases with increasing temperature (because $\Delta\chi$ decreases), then since the characteristic spacing of phase segregated BCP domains, L, is proportional to χ_{AB}^{α} (for instance, α is 1/6 for strongly segregated systems) [46, 47], one would expect L to decrease with an increasing temperature. From Table 5.2, as the CO_2 annealing temperature increases from 60 to 116 °C, the values of both L_1 and L_2 slightly decrease. However, this decrease is within the experimental error range and is therefore inconclusive.

5.5 Conclusions

We demonstrate that supercritical CO_2 induces phase segregation in PEO-b-PFOMA (5k/52k) diblock copolymer thin films. The diblock films remain disordered in vacuum within the temperature range of 80-180 °C. In supercritical CO_2 at 13.9 MPa, between 60 and 116 °C, the diblock films are ordered, with an equilibrium structure of PEO spheres embedded in the matrix of PFOMA. However at 145 °C, the diblock films are disordered. This change of morphology suggests a T_{ODT} between 116 and 145 °C. Regression of the swelling isotherms of PFOMA and PEO homopolymers in CO_2 with the Sanchez-Lacombe equation of state proves that as the temperature increases, $\Delta\chi = |\chi_{\mathrm{PFOMA-CO_2}} - \chi_{\mathrm{PEO-CO_2}}|$ decreases significantly. The CO_2 induced phase segregation is due to the selectivity of CO_2 toward the PFOMA block (large $\Delta\chi$), whereas the effect of dilution ϕ must be minor, as it is in the opposite direction of the experimental observations. At high temperatures, the preferential swelling becomes small enough ($\Delta\chi$ becomes small) that CO_2 no longer induces a transition to the ordered state.

5.6 Bibliography

[1] Segalman, R. A. *Materials Science and Engineering R-Reports* **2005**, *48*(6), 191–226.

[2] Fasolka, M. J.; Mayes, A. M. *Annual Review of Materials Research* **2001**, *31*, 323–355.

[3] Thurn-Albrecht, T.; Schotter, J.; Kastle, C. A.; Emley, N.; Shibauchi, T.; Krusin-Elbaum, L.; Guarini, K.; Black, C. T.; Tuominen, M. T.; Russell, T. P. *Science* **2000**, *290*(5499), 2126–2129.

[4] Sundrani, D.; Darling, S. B.; Sibener, S. J. *Langmuir* **2004**, *20*(12), 5091–5099.

[5] Bodycomb, J.; Funaki, Y.; Kimishima, K.; Hashimoto, T. *Macromolecules* **1999**, *32*(6), 2075–2077.

[6] Albalak, R. J.; Thomas, E. L.; Capel, M. S. *Polymer* **1997**, *38*(15), 3819–3825.

[7] Li, Y.; Meli, L.; Lim, K. T.; Johnston, K. P.; Green, P. F. *Macromolecules* **2006**, *39*(20), 7044–7054.

[8] DeSimone, J. M. *Science* **2002**, *297*(5582), 799–803.

[9] Pai, R. A.; Humayun, R.; Schulberg, M. T.; Sengupta, A.; Sun, J. N.; Watkins, J. J. *Science* **2004**, *303*(5657), 507–510.

[10] Vogt, B. D.; Brown, G. D.; RamachandraRao, V. S.; Watkins, J. J. *Macromolecules* **1999**, *32*(23), 7907–7912.

[11] Vogt, B. D.; RamachandraRao, V. S.; Gupta, R. R.; Lavery, K. A.; Francis, T. J.; Russell, T. P.; Watkins, J. J. *Macromolecules* **2003**, *36*(11), 4029–4036.

[12] Watkins, J. J.; Brown, G. D.; RamachandraRao, V. S.; Pollard, M. A.; Russell, T. P. *Macromolecules* **1999**, *32*(23), 7737–7740.

[13] RamachandraRao, V. S.; Gupta, R. R.; Russell, T. P.; Watkins, J. J. *Macromolecules* **2001**, *34*(23), 7923–7925.

[14] Arceo, A.; Green, P. F. *Journal of Physical Chemistry B* **2005**, *109*(15), 6958–6962.

[15] Lim, K. T.; Lee, M. Y.; Moon, M. J.; Lee, G. D.; Hong, S. S.; Dickson, J. L.; Johnston, K. P. *Polymer* **2002**, *43*(25), 7043–7049.

[16] Arnold, M. E.; Nagai, K.; Freeman, B. D.; Spontak, R. J.; Betts, D. E.; DeSimone, J. M.; Pinnau, I. *Macromolecules* **2001**, *34*(16), 5611–5619.

[17] Madsen, L. A. *Macromolecules* **2006**, *39*(4), 1483–1487.

[18] Bates, F. S.; Fredrickson, G. H. *Annual Review of Physical Chemistry* **1990**, *41*, 525–557.

[19] Loo, Y. L.; Register, R. A.; Ryan, A. J. *Physical Review Letters* **2000**, *84*(18), 4120–4123.

[20] Sirard, S. M.; Green, P. F.; Johnston, K. P. *Journal of Physical Chemistry B* **2001**, *105*(4), 766–772.

[21] Green, P. F. *Journal of Polymer Science Part B-Polymer Physics* **2003**, *41*(19), 2219–2235.

[22] Li, Y.; Loo, Y. L.; Register, R. A.; Green, P. F. *Macromolecules* **2005**, *38*(18), 7745–7753.

[23] Shull, K. R. *Macromolecules* **1996**, *29*(26), 8487–8491.

[24] Xu, T.; Hawker, C. J.; Russell, T. P. *Macromolecules* **2005**, *38*(7), 2802–2805.

[25] Segalman, R. A.; Hexemer, A.; Hayward, R. C.; Kramer, E. J. *Macromolecules* **2003**, *36*(9), 3272–3288.

[26] Reiter, G.; Sommer, J. U. *Physical Review Letters* **1998**, *80*(17), 3771–3774.

[27] Lin, Z. Q.; Kim, D. H.; Wu, X. D.; Boosahda, L.; Stone, D.; LaRose, L.; Russell, T. P. *Advanced Materials* **2002**, *14*(19), 1373–1376.

[28] Reiter, G.; Castelein, G.; Sommer, J. U.; Rottele, A.; Thurn-Albrecht, T. *Physical Review Letters* **2001**, *8722*(22), 4.

[29] Shibayama, M.; Hashimoto, T.; Kawai, H. *Macromolecules* **1983**, *16*(1), 16–28.

[30] Reiter, G. *Journal of Polymer Science Part B-Polymer Physics* **2003**, *41*(16), 1869–1877.

[31] Sirard, S. M.; Ziegler, K. J.; Sanchez, I. C.; Green, P. F.; Johnston, K. P. *Macromolecules* **2002**, *35*(5), 1928–1935.

[32] Sanchez, I. C.; Lacombe, R. H. *Journal of Physical Chemistry* **1976**, *80*(21), 2352–2362.

[33] Sanchez, I. C.; Lacombe, R. H. *Macromolecules* **1978**, *11*(6), 1145–1156.

[34] RamachandraRao, V. S.; Watkins, J. J. *Macromolecules* **2000**, *33*(14), 5143–5152.

[35] Gourgouillon, D.; da Ponte, M. N. *Physical Chemistry Chemical Physics* **1999**, *1*(23), 5369–5375.

[36] Liu, D. H.; Li, H. B.; Noon, M. S.; Tomasko, D. L. *Macromolecules* **2005**, *38*(10), 4416–4424.

[37] Sanchez, I. C.; Stone, M. T. In *Polymer Blends Volume I: Formulation*; Paul, D. R., Bucknall, C. B., Eds., Vol. 1; John Wiley & Sons, Inc: New York, 2000; page 15.

[38] Luna-Barcenas, G. *work to be published.*

[39] Harrison, K. L.; Johnston, K. P.; Sanchez, I. C. *Langmuir* **1996**, *12*(11), 2637–2644.

[40] Condo, P. D.; Sumpter, S. R.; Lee, M. L.; Johnston, K. P. *Industrial & Engineering Chemistry Research* **1996**, *35*(4), 1115–1123.

[41] O'Neill, M. L.; Cao, Q.; Fang, R.; Johnston, K. P.; Wilkinson, S. P.; Smith, C. D.; Kerschner, J. L.; Jureller, S. H. *Industrial and Engineering Chemistry Research* **1998**, *37*(8), 3067–3079.

[42] Panayiotou, C. *Fluid Phase Equilibria* **1997**, *131*(1-2), 21–35.

[43] Weidner, E.; Wiesmet, V.; Knez, Z.; Skerget, M. *Journal of Supercritical Fluids* **1997**, *10*(3), 139–147.

[44] Guadagno, T.; Kazarian, S. G. *Journal of Physical Chemistry B* **2004**, *108*(37), 13995–13999.

[45] Daneshvar, M.; Kim, S.; Gulari, E. *Journal of Physical Chemistry* **1990**, *94*(5), 2124–2128.

[46] Bates, F. S. *Science* **1991**, *251*(4996), 898–905.

[47] Matsen, M. W.; Bates, F. S. *Macromolecules* **1996**, *29*(4), 1091–1098.

[48] Hanley, K. J.; Lodge, T. P. *Journal of Polymer Science Part B-Polymer Physics* **1998**, *36*(17), 3101–3113.

[49] Robard, A.; Patterson, D.; Delmas, G. *Macromolecules* **1977**, *10*(3), 706–708.

Chapter 6

Summary

6.1 Conclusions

This dissertation is devoted to understand the effects of high pressure CO_2 on the polymer systems by using computational methods.

In Chapter 2, we introduce the methodology used in this dissertation. The combination of gradient theory of inhomogeneous systems and Sanchez-Lacombe Equation of State is used to calculate the interfacial properties.

In Chapter 3, we show analytically that surface adsorption on an attractive surface is proportional to the compressibility of the fluid. We have also investigated numerically the sorption of supercritical CO_2 on poly(dimethylsiloxane) and polyisobutylene, and supercritical 1,1-difluoroethane on polystyrene. By calculating the Gibbs adsorption and adsorption layer thickness of the supercritical fluids, we find in all cases (different substrates, different supercritical fluids) that maximum adsorption occurs when the supercritical fluid is near its compressibility maximum.

In Chapter 4, we calculate the interfacial density profile, interfacial thickness and interfacial tension between the two polymers with and without the supercritical fluid. We find that the interfacial tension is decreased and

the interfacial thickness is increased with high pressure supercritical fluid for the ternary systems we have investigated.

In Chapter 5, we examine the morphological structures of asymmetric poly(ethylene oxide)-b-poly(1,1'-dihydroperflurooctyl methacrylate) (PEO-b-PFOMA) thin films upon annealing in supercritical CO_2. The strong affinity between PFOMA and CO_2 is found to induce phase segregation when annealing PEO-b-PFOMA films at the same temperature as compared with vacuum annealing under the same temperature. The results are explained based on the relative interaction parameters, $\chi_{\mathrm{PFOMA-CO_2}}$ and $\chi_{\mathrm{PEO-CO_2}}$.

6.2 Future Work

Future work would be on the interaction between supercritical fluid with polymer on the polymer/substrate side.

More work can be expected to investigate the interaction between supercritical fluids and polymer systems with field-theoretical simulations [1]. Field-based computer simulations is an alternative way to model polymer fluids. In field-based theoretical methods, the connectivity of mers in a polymer is considered. The technique represents a powerful tool to examine complex phenomena, such as the dynamical effects of solvent on the immiscible polymers and the solvent effect on the block copolymers.

6.3 Bibliography

[1] Fredrickson, G. H. Vol. 134 of *International series of monographs on physics;* Clarendon Press: Oxford ; New York, 2006.

Bibliography

[1] Albalak, R. J., Thomas, E. L., and Capel, M. S. *Polymer 38*, 15 (1997), 3819–3825.

[2] Anderson, K. L., Wescott, J. T., Carver, T. J., and Windle, A. H. *Materials Science and Engineering a-Structural Materials Properties Microstructure and Processing 365*, 1-2 (2004), 14–24.

[3] Arceo, A., and Green, P. F. *Journal of Physical Chemistry B 109*, 15 (2005), 6958–6962.

[4] Arnold, M. E., Nagai, K., Freeman, B. D., Spontak, R. J., Betts, D. E., DeSimone, J. M., and Pinnau, I. *Macromolecules 34*, 16 (2001), 5611–5619.

[5] Bates, F. S. *Science 251*, 4996 (1991), 898–905.

[6] Bates, F. S., and Fredrickson, G. H. *Annual Review of Physical Chemistry 41* (1990), 525–557.

[7] Benkoski, J. J., Fredrickson, G. H., and Kramer, E. J. *Journal of Polymer Science Part B-Polymer Physics 40*, 20 (2002), 2377–2386.

[8] Besancon, B. M., Soles, C. L., and Green, P. F. *Physical Review Letters 97*, 5 (2006).

[9] Bodycomb, J., Funaki, Y., Kimishima, K., and Hashimoto, T. *Macromolecules 32*, 6 (1999), 2075–2077.

[10] Bongiorno, V., and Davis, H. T. *Physical Review A 12*, 5 (1975), 2213–2224.

[11] Brandrup, J., Immergut, E. H., and Grulke, E. A. 4th ed. 1999.

[12] Buxton, G. A., and Balazs, A. C. *Interface Science 11*, 2 (2003), 175–186.

[13] Cahn, J. W. *Journal Of Chemical Physics 66*, 8 (1977), 3667–3672.

[14] Cahn, J. W., and Hilliard, J. E. *Journal of Chemical Physics 28* (1958), 258–67.

[15] Chang, S. H., Park, S. C., and Shim, J. J. *Journal of Supercritical Fluids 13*, 1-3 (1998), 113–119.

[16] Cintavey, L. A., Clarson, S. J., Husband, D. M., De Brabander, G. N., and Boyd, J. T. *Journal of Applied Polymer Science 76*, 9 (2000), 1448–1456.

[17] Condo, P. D., Sumpter, S. R., Lee, M. L., and Johnston, K. P. *Industrial & Engineering Chemistry Research 35*, 4 (1996), 1115–1123.

[18] Daneshvar, M., Kim, S., and Gulari, E. *Journal of Physical Chemistry 94*, 5 (1990), 2124–2128.

[19] DeSimone, J. M. *Science 297*, 5582 (2002), 799–803.

[20] Elkovitch, M. D., Tomasko, D. L., and Lee, L. J. *Polymer Engineering and Science 39*, 10 (1999), 2075–2084.

[21] Eugene, H., and Yukiko, T. *The Journal of Chemical Physics 56*, 7 (1972), 3592–3601.

[22] Fasolka, M. J., and Mayes, A. M. *Annual Review of Materials Research 31* (2001), 323–355.

[23] Fleming, G. K., and Koros, W. J. *Macromolecules 19*, 8 (1986), 2285–2291.

[24] Frank, C. W., Rao, V., Despotopoulou, M. M., Pease, R. F. W., Hinsberg, W. D., Miller, R. D., and Rabolt, J. F. *Science 273*, 5277 (1996), 912–915.

[25] Fredrickson, G. H. vol. 134 of *International series of monographs on physics*. Clarendon Press, Oxford ; New York, 2006.

[26] Garg, A., Gulari, E., and Manke, C. W. *Macromolecules 27*, 20 (1994), 5643–5653.

[27] Gourgouillon, D., and da Ponte, M. N. *Physical Chemistry Chemical Physics 1*, 23 (1999), 5369–5375.

[28] Green, P. F. *Journal of Polymer Science Part B-Polymer Physics 41*, 19 (2003), 2219–2235.

[29] Guadagno, T., and Kazarian, S. G. *Journal of Physical Chemistry B 108*, 37 (2004), 13995–13999.

[30] Haire, K. R., and Windle, A. H. *Computational and Theoretical Polymer Science 11*, 3 (2001), 227–240.

[31] Hanley, K. J., and Lodge, T. P. *Journal of Polymer Science Part B-Polymer Physics 36*, 17 (1998), 3101–3113.

[32] Harrison, K. L., Johnston, K. P., and Sanchez, I. C. *Langmuir 12*, 11 (1996), 2637–2644.

[33] Helfand, E., and Sapse, A. M. *Journal of Chemical Physics 62*, 4 (1975), 1327–1331.

[34] Helfand, E., and Tagami, Y. *Journal of Polymer Science Part B-Polymer Physics 34*, 12 (1996), 1947–1952.

[35] Hong, K. M., and Noolandi, J. *Macromolecules 14*, 3 (1981), 736–742.

[36] Hong, K. M., and Noolandi, J. *Macromolecules 14*, 3 (1981), 727–736.

[37] Koga, T., Jerome, J., Rafailovich, M. H., Chu, B., Douglas, J., and Satija, S. *Advances in Colloid and Interface Science 128* (2006), 217–226.

[38] Koga, T., Jerome, J. L., Seo, Y. S., Rafailovich, M. H., Sokolov, J. C., and Satija, S. K. *Langmuir 21*, 14 (2005), 6157–6160.

[39] Koga, T., Seo, Y. S., Shin, K., Zhang, Y., Rafailovich, M. H., Sokolov, J. C., Chu, B., and Satija, S. K. *Macromolecules 36*, 14 (2003), 5236–5243.

[40] Koga, T., Seo, Y.-S., Zhang, Y., Shin, K., Kusano, K., Nishikawa, K., Rafailovich, M. H., Sokolov, J. C., Chu, B., Peiffer, D., Occhiogrosso, R., and Satija, S. K. *Physical Review Letters 89*, 12 (2002), 125506/1–125506/4.

[41] Li, H. B., Lee, L. J., and Tomasko, D. L. *Industrial and Engineering Chemistry Research 43*, 2 (2004), 509–514.

[42] Li, Y., Loo, Y. L., Register, R. A., and Green, P. F. *Macromolecules 38*, 18 (2005), 7745–7753.

[43] Li, Y., Meli, L., Lim, K. T., Johnston, K. P., and Green, P. F. *Macromolecules 39*, 20 (2006), 7044–7054.

[44] Lim, K. T., Lee, M. Y., Moon, M. J., Lee, G. D., Hong, S. S., Dickson, J. L., and Johnston, K. P. *Polymer 43*, 25 (2002), 7043–7049.

[45] Lin, Z. Q., Kim, D. H., Wu, X. D., Boosahda, L., Stone, D., LaRose, L., and Russell, T. P. *Advanced Materials 14*, 19 (2002), 1373–1376.

[46] Liu, D. H., Li, H. B., Noon, M. S., and Tomasko, D. L. *Macromolecules 38*, 10 (2005), 4416–4424.

[47] Loo, Y. L., Register, R. A., and Ryan, A. J. *Physical Review Letters 84*, 18 (2000), 4120–4123.

[48] Luna-Barcenas, G. *work to be published*.

[49] Madsen, L. A. *Macromolecules 39*, 4 (2006), 1483–1487.

[50] Mark, J. E. 1 st ed. New York, 1999.

[51] Matsen, M. W., and Bates, F. S. *Macromolecules 29*, 4 (1996), 1091–1098.

[52] McHugh, M. A., and Krukonis, V. 2nd ed. Boston, 1994.

[53] Merkel, T. C., Bondar, V. I., Nagai, K., Freeman, B. D., and Pinnau, I. *Journal of Polymer Science Part B-Polymer Physics 38*, 3 (2000), 415–434.

[54] Nadakatti, S. M., Kim, J. H., and Stern, S. A. *Journal of Membrane Science 108*, 3 (1995), 279–291.

[55] Nalawade, S. P., Picchioni, F., and Janssen, L. *Progress in Polymer Science 31*, 1 (2006), 19–43.

[56] O'Neill, M. L., Cao, Q., Fang, R., Johnston, K. P., Wilkinson, S. P., Smith, C. D., Kerschner, J. L., and Jureller, S. H. *Industrial and Engineering Chemistry Research 37*, 8 (1998), 3067–3079.

[57] Pai, R. A., Humayun, R., Schulberg, M. T., Sengupta, A., Sun, J. N., and Watkins, J. J. *Science 303*, 5657 (2004), 507–510.

[58] Palermo, E., Si, M., Occhiogrosso, R., Berndt, C., Rudomen, G., and Rafailovich, M. *Macromolecules 38*, 22 (2005), 9180–9186.

[59] Panayiotou, C. *Fluid Phase Equilibria 131*, 1-2 (1997), 21–35.

[60] Pham, J. Q., and Green, P. F. *Macromolecules 36*, 5 (2003), 1665–1669.

[61] Pope, D. S., Sanchez, I. C., Koros, W. J., and Fleming, G. K. *Macromolecules 24*, 8 (1991), 1779–1783.

[62] Poser, C. I. Ph. d. thesis, University of Massachusetts, 1980.

[63] Poser, C. I., and Sanchez, I. C. *Journal of Colloid and Interface Science 69*, 3 (1979), 539–548.

[64] Poser, C. I., and Sanchez, I. C. *Macromolecules 14*, 2 (1981), 361–70.

[65] RamachandraRao, V. S., Gupta, R. R., Russell, T. P., and Watkins, J. J. *Macromolecules 34*, 23 (2001), 7923–7925.

[66] RamachandraRao, V. S., and Watkins, J. J. *Macromolecules 33*, 14 (2000), 5143–5152.

[67] Reiter, G. *Journal of Polymer Science Part B-Polymer Physics 41*, 16 (2003), 1869–1877.

[68] Reiter, G., Castelein, G., Sommer, J. U., Rottele, A., and Thurn-Albrecht, T. *Physical Review Letters 8722*, 22 (2001), 4.

[69] Reiter, G., and Sommer, J. U. *Physical Review Letters 80*, 17 (1998), 3771–3774.

[70] Robard, A., Patterson, D., and Delmas, G. *Macromolecules 10*, 3 (1977), 706–708.

[71] Rowlinson, J. S. *Journal of Statistical Physics 20*, 2 (1979), 197–244.

[72] Royer, J. R., DeSimone, J. M., and Khan, S. A. *Macromolecules 32*, 26 (1999), 8965–8973.

[73] Sanchez, I. C. *Journal of Macromolecular Science-Physics B17*, 3 (1980), 565–589.

[74] Sanchez, I. C., and Lacombe, R. H. *Journal of Physical Chemistry 80*, 21 (1976), 2352–2362.

[75] Sanchez, I. C., and Lacombe, R. H. *Macromolecules 11*, 6 (1978), 1145–1156.

[76] Sanchez, I. C., and Stone, M. T. In *Polymer Blends Volume I: Formulation*, D. R. Paul and C. B. Bucknall, Eds., vol. 1. John Wiley & Sons, Inc, New York, 2000, p. 15.

[77] Schnell, R., Stamm, M., and Creton, C. *Macromolecules 31*, 7 (1998), 2284–2292.

[78] Segalman, R. A. *Materials Science and Engineering R-Reports 48*, 6 (2005), 191–226.

[79] Segalman, R. A., Hexemer, A., Hayward, R. C., and Kramer, E. J. *Macromolecules 36*, 9 (2003), 3272–3288.

[80] Shibayama, M., Hashimoto, T., and Kawai, H. *Macromolecules 16*, 1 (1983), 16–28.

[81] Shim, J. J., and Johnston, K. P. *Aiche Journal 35*, 7 (1989), 1097–1106.

[82] Shull, K. R. *Macromolecules 29*, 26 (1996), 8487–8491.

[83] Sirard, S. M., Green, P. F., and Johnston, K. P. *Journal of Physical Chemistry B 105*, 4 (2001), 766–772.

[84] Sirard, S. M., Gupta, R. R., Russell, T. P., Watkins, J. J., Green, P. F., and Johnston, K. P. *Macromolecules 36*, 9 (2003), 3365–3373.

[85] Sirard, S. M., Ziegler, K. J., Sanchez, I. C., Green, P. F., and Johnston, K. P. *Macromolecules 35*, 5 (2002), 1928–1935.

[86] Sundrani, D., Darling, S. B., and Sibener, S. J. *Langmuir 20*, 12 (2004), 5091–5099.

[87] Thurn-Albrecht, T., Schotter, J., Kastle, C. A., Emley, N., Shibauchi, T., Krusin-Elbaum, L., Guarini, K., Black, C. T.,

Tuominen, M. T., and Russell, T. P. *Science 290*, 5499 (2000), 2126–2129.

[88] Tomasko, D. L., Li, H. B., Liu, D. H., Han, X. M., Wingert, M. J., Lee, L. J., and Koelling, K. W. *Industrial and Engineering Chemistry Research 42*, 25 (2003), 6431–6456.

[89] Vogt, B. D., Brown, G. D., RamachandraRao, V. S., and Watkins, J. J. *Macromolecules 32*, 23 (1999), 7907–7912.

[90] Vogt, B. D., RamachandraRao, V. S., Gupta, R. R., Lavery, K. A., Francis, T. J., Russell, T. P., and Watkins, J. J. *Macromolecules 36*, 11 (2003), 4029–4036.

[91] Walker, T. A., Colina, C. M., Gubbins, K. E., and Spontak, R. J. *Macromolecules 37*, 7 (2004), 2588–2595.

[92] Walker, T. A., Melnichenko, Y. B., Wignall, G. D., and Spontak, R. J. *Macromolecules 36*, 12 (2003), 4245–4249.

[93] Walker, T. A., Raghavan, S. R., Royer, J. R., Smith, S. D., Wignall, G. D., Melnichenko, Y., Khan, S. A., and Spontak, R. J. *Journal of Physical Chemistry B 103*, 26 (1999), 5472–5476.

[94] Wang, X., and Sanchez, I. C. *Langmuir 22*, 22 (2006), 9251–9253.

[95] Watkins, J. J., Brown, G. D., RamachandraRao, V. S., Pollard, M. A., and Russell, T. P. *Macromolecules 32*, 23 (1999), 7737–7740.

[96] Weidner, E., Wiesmet, V., Knez, Z., and Skerget, M. *Journal of Supercritical Fluids 10*, 3 (1997), 139–147.

[97] Xu, T., Hawker, C. J., and Russell, T. P. *Macromolecules 38*, 7 (2005), 2802–2805.

[98] Yeo, S. D., and Kiran, E. *Journal of Supercritical Fluids 34*, 3 (2005), 287–308.

[99] Yoon, K. S., Pak, H., Lee, J. W., and Chang, T. *Bulletin of the Korean Chemical Society 15*, 3 (1994), 214–221.

[100] Zhang, X. G., Pham, J. Q., Ryza, N., Green, P. F., and Johnston, K. P. *Journal of Vacuum Science and Technology B 22*, 2 (2004), 818–825.

[101] Ziemelis, K. *Nature 393*, 6686 (1998), 619–620.

Vita

Xiaochu Wang, son of Mengqun Wang and Jinmei Chu, was born on October 23 1979, in Yongkang, Zhejiang Province, P. R. China. He attended Zhejiang University in Hangzhou, China and got his Bachelor degree of Control Science and Engineering in June 2000. He got his Master degree of Control Science and Engineering also from Zhejiang University in June 2003. Mr. Wang was admitted to graduate school at the University of Texas at Austin in September 2003.

Permanent address: 2200 Willow Creek Dr., Apt 1201
Austin, Texas 78741

This dissertation was typeset with LaTeX[†] by the author.

[†]LaTeX is a document preparation system developed by Leslie Lamport as a special version of Donald Knuth's TeX Program.